

Acknowledgments

Sherman Beychok was to have written this chapter, but because of the pressures of other work, he asked me to join him in it. I agreed, largely for the pleasure of working with him. The demands on his time and attention grew, however, and in the end he felt unable to do justice to this volume in the time available for its completion. Although the words here are therefore mine, his contribution is present throughout, for much of the chapter took shape in the course of our discussions. Being stubborn, I did not always follow good advice, and the resulting flaws are mine alone.

The sardonic skepticism of Phillip Pechukas served a useful purpose, and the assistance of Rhea McDonald in preparing the manuscript was essential.

The support of the New Jersey State Agricultural Experiment Station, The Rutgers University Research Council, and a Biomedical Resources Support Grant are also acknowledged.

[17] Time-Resolved Fluorescence Measurements

By MUGUREL G. BADEA and LUDWIG BRAND

Introduction

During the last decade, fluorescence techniques have been applied to numerous problems in biology and biochemistry. Both intrinsic and extrinsic fluorophores have been used to obtain information about proteins, nucleic acids, membranes and other biological materials. The increasing interest in the application of fluorescence methods in the life sciences has led to a continuing development of new instrumental techniques and procedures for data analysis. Nanosecond fluorometry represents an area of particularly intense activity. Ten years ago, the measurement of fluorescence decay times was still in its infancy and it was difficult, if not impossible, to measure and analyze multiexponential decay curves with any degree of confidence. Today, this situation has been completely altered and nanosecond decay data, nanosecond time-resolved emission spectra, and the decay of the emission anisotropy can readily be obtained and analyzed. As a consequence, complex excited state interactions have become better understood and have been used to probe biological microenvironments.

It would be difficult to cover all the advances in experimental techniques that have been made in the last ten years and this will not be attempted. Numerous specialized topics such as differential fluorimetry, solute perturbation fluorescence, stopped flow fluorescence, fluorescence circular dichroism, have been or will be covered in other chapters in these volumes. Topics to be covered here include the following: advances in the instrumentation and procedures for data analysis required for nanosecond fluorometry; potentials of nanosecond time-dependent fluorescence emis-

sion spectroscopy, and nanosecond time-dependent emission anisotropy. In addition the treatment of decay data to obtain information regarding excited state interactions will be discussed.

The relations between fluorescence, excited state interactions, and probe environment are the themes to be emphasized. Reactions that occur in the excited state can either be inferred from or directly measured by the parameters characterizing the luminescence.¹

There are a large number of excited state interactions that can occur prior to or can compete with fluorescence emission. These include vibrational relaxation of the photo-excited state, internal conversion and intersystem crossing, conformational change, hydrogen bonding, orientational relaxation in fluid media, proton transfer, electron ejection, exciplex and excimer formation, excited state charge transfer complexes, and nonradiative energy transfer which can be singlet-singlet or triplet-triplet. While this list is not complete, it does indicate the variety of excited state interactions that are known to exist and that have been studied in some detail. The extent to which these interactions take place will depend on the character of the fluorophore, on other molecules in the vicinity, and on general environmental factors, such as the solvent, the viscosity, and the temperature. It is desirable that the excited state interactions of a fluorescence probe first be characterized in detail in model solvent systems. In this way, when the fluorophore is used to probe a biological system, the information derived may be interpreted on a firm basis to give information about the microenvironment.

The shortest relaxation times measured for many of the excited state interactions indicated above are on the picosecond time scale. An excellent review of the published data on the picosecond time scale has been presented by Eisinger.¹ In many cases of interest in biology, the environmental conditions are or can be made to be such that most excited state processes, including fluorescence, occur on the nanosecond time scale. The measured fluorescence decay time τ reflects the competition between fluorescence emission and other excited state reactions or quenching. If all other deexcitation channels are suppressed, then all the quanta absorbed will be emitted as fluorescence. Under these conditions the fluorescence decay time approaches the natural lifetime τ_0 . The natural lifetime is related to the probability of the transition to the ground state and is often on the order of nanoseconds. The quantum yield approaches unity as the measured lifetime approaches the natural lifetime. These relations are summarized below.

$$q = \frac{\tau_m}{\tau_0} \quad \tau_0 = \frac{1}{k_f} \quad \frac{1}{k_f + k_{(\text{other})}} \quad (1)$$

¹ K. B. Eisinger, *Annu. Rev. Phys. Chem.* **28**, 207 (1977).

where τ_m and τ_0 are the measured and natural lifetimes respectively, q is the quantum yield, and k_f and $k_{(\text{other})}$ are the rate constants for the fluorescence and nonfluorescence decay to the ground state, respectively.

The microenvironment which biomolecules and bioaggregates create around fluorophores can thus be probed through nanosecond fluorescence measurements. These measurements will provide information about processes that may be occurring concomitant with fluorescence. Changes in the rates of these processes can be correlated with changes in the biologically relevant parameters influencing them. The power of nanosecond fluorescence techniques lie in determining the *dynamics* of conformational changes of, or interaction between, biomacromolecules and biological macroassemblies. In some instances, nature has provided us with "built-in" fluorescence probes. Examples include the aromatic amino acids, especially tryptophan and tyrosine. Other examples include fluorescent coenzymes, such as pyridine nucleotides, pyridoxal phosphate, or flavins. In other cases, it is necessary to add a probe attached covalently or noncovalently to the system.

Our aim here is to provide an overview of the nanosecond fluorescence field at its present stage of development. As mentioned above, this section will not be comprehensive, but will rather be selective reflecting the experience (and bias!) of the authors. A comparative appraisal of the various instrumental techniques used in nanosecond fluorometry will be provided. Since suitable procedures for analysis of the data are as essential in nanosecond fluorometry as the instrumentation itself, the conceptual basis of the procedures for elimination of the convolution artifacts and thus obtaining the true fluorescence relaxation times will be described. The experimental procedures for performing time-resolved fluorescence measurements, i.e., time-resolved emission spectra (TRES) and decay of the emission anisotropy (DEA) will be explicitly dealt with. Finally, some selected examples of ways to handle complex decay data will be presented.

Fluorescence Decay Instrumentation

The most significant advances in fluorometry during the last decade are those that have been made in regard to the instrumentation required for fluorescence decay studies. Fluorescence lifetimes are usually of the order of nanoseconds, and, until recently, this short time scale made the measurements difficult. The development of the instrumental techniques required for decay measurements has proceeded in two directions.

The transient fluorescence properties of a molecular system can be studied by observing its response to either a continuous, high frequency

modulated excitation or to a series of discrete, repetitive, short exciting pulses. In either case the desired information regarding fluorescence decay laws is extracted from the modification of the time profile of the exciting signal due to the lag introduced by the finite duration of the excited state.

Continuous Response Technique. In the literature, this method of determining the kinetics of the fluorescent decay is known as the "phase shift method." The kinetic information is usually obtained by measuring the phase shift (δ) between the excitation wave form and the corresponding fluorescence response wave form.² If a homogeneous population of *monoexponentially* decaying molecules is excited with sinusoidal modulated light with frequency f , then the decay constant τ is related to δ and f according to the formula

$$\tan \delta = 2\pi f\tau \quad (2)$$

In this case, the decay constant can also be obtained from the degree of modulation of the fluorescence relative to that of the exciting light given by

$$m = \text{relative modulation} = \frac{\text{modulation of fluorescence}}{\text{modulation of excitation}} \quad (3)$$

$$\frac{(F_{\max} - F_{\min})/(F_{\max} + F_{\min})}{(E_{\max} - E_{\min})/(E_{\max} + E_{\min})} = \frac{1}{(1 + 4\pi f\tau)^{1/2}} = \cos \delta$$

where F_{\max} is maximal fluorescence and F_{\min} is minimal fluorescence

The modulation frequency f is chosen to yield maximum measuring accuracy for both $\tan \delta$ and m . This happens when $f \sim 1/2\pi\tau$ which for decay constants in the range of 3–50 nsec corresponds to frequencies between 3 and 50 MHz.

Both Eqs. (2) and (3) are valid only for an emitting molecular system which decays monoexponentially, an assumption implicit in their derivation. A sufficient check for the validity of this assumption is the equality of the decay constants obtained from each equation, respectively. If the assumption is not valid, the decay constant measured by the degree of modulation will almost always be larger than that determined from the phase shift.²

In the multiexponential case the equations corresponding to Eqs. (2) and (3) are given by³

² R. D. Spencer and G. Weber, *Ann. N. Y. Acad. Sci.* **158**, 361 (1969).

³ S. R. Schuldinger, D. Spencer, G. Weber, R. Weil, and H. R. Kaback, *J. Biol. Chem.* **250**, 8893 (1975).

$$\tan \bar{\phi} = \frac{\sum_i F_i \sin \phi_i \cos \phi_i}{\sum_i F_i \cos^2 \phi_i} \quad (2')$$

$$\bar{M}^2 = \left(\sum_i F_i \cos^2 \phi_i \right) + \left(\sum_i F_i \sin \phi_i \cos \phi_i \right) \quad (3')$$

where the $\bar{\phi}$ and \bar{M} are the experimentally observed phase lag and relative modulation and ϕ_i and F_i are the phase shift and fractional contribution of the i th component. To extract the individual parameters of an n -component system, n separate measurements of $\bar{\phi}$ and $\pm\bar{M}$ should be performed at n modulation frequencies.

Ideally, in order to ascertain the multicomponent nature of a given fluorescence decay the phase fluorimeter should possess the capability of a continuous variable frequency. Then the fluorescence intensity time profile could be obtained as the Fourier transform of the phase shift data taken at various frequencies.

While there are still technical difficulties associated with variable frequency measurements, good progress in this direction is being made.^{4,5} Application of these techniques to the resolution of multi or nonexponential decay systems may be expected in the near future. At the time of writing, much of the work in this area has been performed on decay instruments based on pulse techniques (see below). Wherever the monoexponential character of the decay is firmly established the continuous response methods have excellent subnanosecond sensitivity and accuracy coupled with a relatively fast data acquisition. Several technical improvements^{2,4,6} especially in the procedures used for phase detection have resulted in instruments capable of measuring differences of 0.1 nsec with an accuracy of 0.03 nsec between two decay constants each less than 1 nsec.² Suitable instrumentation for phase fluorometry is now available commercially.⁷

Discrete Response Technique. Significant advances have been made in the development of several types of nanosecond fluorimeters based on pulse techniques such that this approach can be used to resolve complex fluorescence decay data. The pulse technique has also been used to obtain nanosecond time-resolved emission spectra and nanosecond time-resolved emission anisotropy data. Since pulse methods are used in our own laboratories their use will be emphasized here.

⁴ M. Hauser and G. Heidt, *Rev. Sci. Instrum.* **46**, 470 (1975).

⁵ F. E. Lytle, J. F. Eng, J. M. Harris, T. D. Harris, and R. E. Santini, *Anal. Chem.* **47**, 571 (1975).

⁶ V. E.-P. Resewitz and E. Lippert, *Ber. Bunsenges. Phys. Chem.* **78**, 1227 (1974).

⁷ SLM Instruments, Champaign, Illinois.

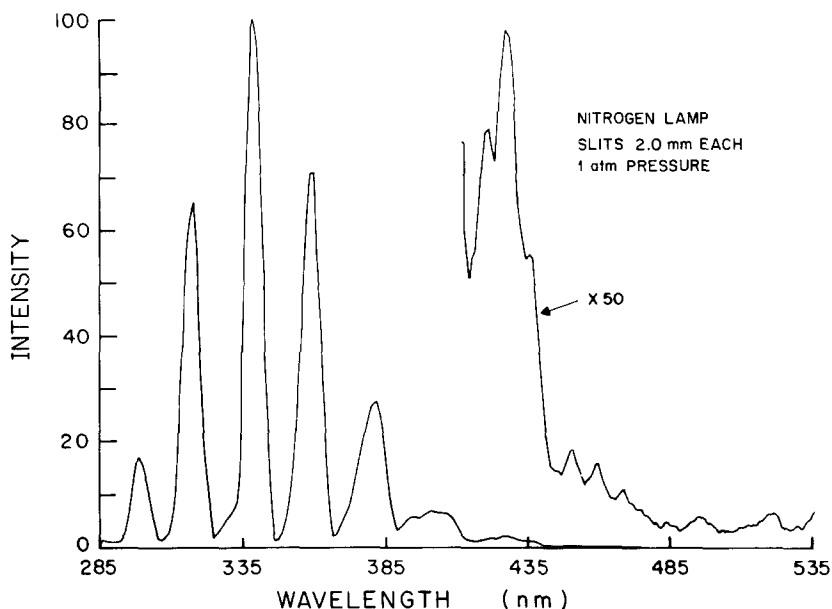


FIG. 1. Relative intensity distribution of a 1 atm nitrogen nanosecond flash lamp. The relative intensities from 400 to 530 nm are also shown amplified 50-fold. The emission was observed through a Bausch and Lomb No. 33-86-44 monochromator (33 Å/mm). The entrance and exit slits of the monochromator were set at 2 mm.

The pulsed excitation is provided by a nanosecond flash lamp, freerunning or gated at a particular frequency. The frequency is usually less than 50 kHz so that decays as long as 1000 nsec initiated by one flash are not perturbed by the next. It is our experience that gated lamps not only allow a convenient choice of a constant repetition rate but also exhibit improved lamp intensity per flash and pulse shape reproducibility. A thyatron gated nanosecond flash lamp with repetition rates up to 50 kHz is now available commercially from PRA⁸ together with the required power supply. Based on a design due to Ware,⁹ it allows the lamp gas to be changed with ease. Nitrogen gives intense light between 300 and 400 nm (Fig. 1) with lines at 226, 316, 337, 358 and 381 nm. Hydrogen and deuterium (Fig. 2) can be used to obtain excitation further in the ultraviolet. The timing characteristics of typical flash lamps now in use enable one to obtain flash profiles with a width at half-maximum about 2 nsec. Most lamps usually show a moderate tail as seen in Fig. 3. The electromagnetic

⁸ PRA (Photochemical Research Associates Inc.), N6A 5B7. University of Western Ontario, London, Ontario, Canada.

⁹ W. Ware, in "Creation and Detection of the Excited State" (A. A. Lamola, ed.), Vol. 1, Part A, p. 213. Dekker, New York, 1971.

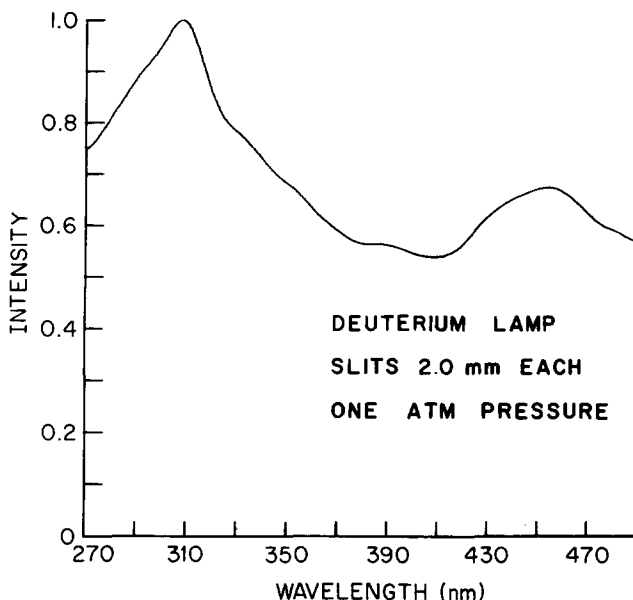


FIG. 2. Relative intensity distribution of a deuterium nanosecond flash lamp. The monochromator is as described in the legend to Fig. 1. The intensity scale is not related to that shown for Fig. 1.

radiation associated with the spark can be picked up by an antenna and used as a timing pulse to trigger the detection system. Alternatively, a suitable timing pulse can be provided by an electron multiplier phototube (an RCA IP28 is commonly used) which views the lamp directly.

Once the sample is excited a variety of methods are available for monitoring the time course of the fluorescence decay. From this point of view, the nanosecond pulse fluorimeters are divided into two general types: (a) those that monitor many photons per pulse and (b) those that monitor only one photon per pulse (monophoton counting instruments). Both these types of instruments usually employ a combination of analog and digital techniques for data acquisition.

In the simplest case, the fluorescence decay of a sample is described by a single exponential:

$$I(t) = I_0 e^{-kt} = I_0 e^{-t/\tau} \quad (4)$$

where k represents the probability of a particular molecule emitting a fluorescence photon following excitation. This probability is assumed to be time independent. The exponential law is obtained by summing the photon contributions of an assembly of potentially fluorescent molecules at each infinitesimal time interval after synchronous excitation. In the

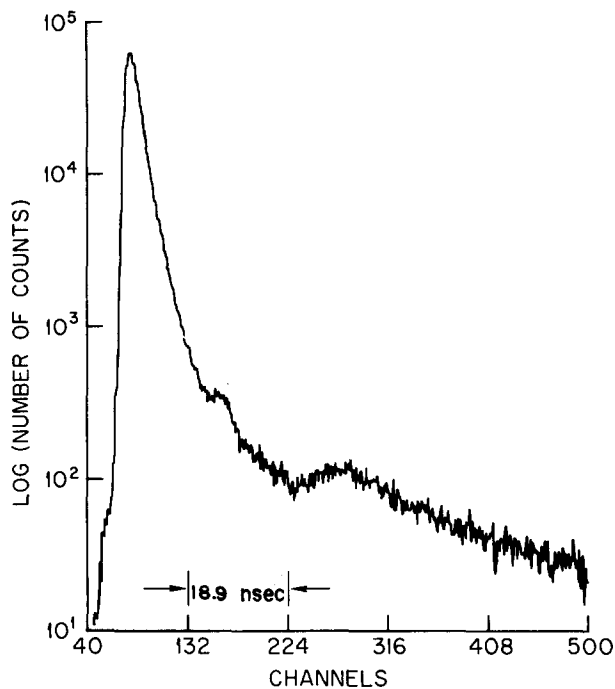


FIG. 3. Typical time-intensity profile of a 1 atm nitrogen flash lamp. There are 0.205 nsec/channel. The ordinate is a logarithmic scale in order to emphasize the tail.

limit of very small time intervals, $I(t)$ is thus proportional to the number of excited molecules making the transition to the ground state at time t after excitation.

At the present time, fast electronic circuitry capable of reproducing the decay of fluorescence light intensity on the nanosecond time scale is not widespread. The first type of existing instrumentation obviates this stringent requirement by prepositioning a constant, narrow time window (aperture) at variable delays after the triggering pulse and integrating the effect produced by the many photons received during the aperture opening. The delay is varied to cover the whole measurable decay curve, and the integration could be performed on various physical quantities proportional to the photon flux, i.e. photocurrent,¹⁰ photovoltage,¹¹ or light emission from a slowly decaying phosphor detector screen.¹² The reader is referred to the original literature for details on these ingenious techniques. The second type of instrumentation concentrates on the time axis

¹⁰ R. G. Bennett, *Rev. Sci. Instrum.* **31**, 1275 (1960).

¹¹ O. J. Steingraber and I. B. Berلمان, *Rev. Sci. Instrum.* **34**, 524 (1963).

¹² J. Yguerabide, *Rev. Sci. Instrum.* **36**, 1734 (1965).

of the decay curve rather than on the intensity. It accepts only one fluorescence photon per exciting flash and times its arrival relative to the latter. The histogram of a large number of such events (i.e., number of photons versus time of arrival) will represent, in the large limit, the actual decay curve. Only the first arriving photon is accepted such that it is essential that the conditions of collection be such that all possible times of arrival are equally represented.⁹ In what follows, the operation and the conditions for proper use of the nanosecond instrumentation will be dealt with in some detail, stressing the respective advantages and disadvantages of the two types of instrumentation mentioned above.

MULTIPLE PHOTONS PER EXCITING PULSE. The block diagram of a typical instrument collecting multiple photons per excited pulse is shown in Fig. 4. It is easily assembled from commercially available units.¹³ The heart of the instrument is a Princeton Applied Research Co., dual channel boxcar averager main frame model 162 fitted with two model 163 sampled integrators which incorporate two Tektronix S-2 sampling heads. One head is used to process successively the fluorescence and the excitation signals coming from a 56 TUVP Amperex photomultiplier which views either the fluorescent sample or the scatterer. The wavelength at which the emission is detected is selected by a monochromator and the excitation is performed through an interference filter. A beam splitter allows the simultaneous monitoring of the fluctuations in excitation by a 56 DUVP 03 photomultiplier whose output is fed into the second S-2 sampling head. By taking the instantaneous ratio of the fluorescence signal to the exciting light signal, the fluorescence decay data is obtained free of any fluctuations in the excitation intensity.¹⁴

The boxcar averaging is a process which involves measuring the amplitude of a particular point on a repetitive signal, integrating the result, and computing a representative average. Specifically, at any chosen time after a triggering signal, the nonadjustable sampling gate of 75 psec, built into the electronic circuitry of the S-2 sample head, opens and records the instantaneous peak amplitude of the repetitive signal. This process is performed a chosen number of times and the result averaged in a memory unit contained in the Model 163 sampled integrator. Then, controls from the Model 162 main frame allow a manual or an automatic new choice of the delay time (after the trigger) when the sampling gate opens and the process is repeated. The range to be scanned can be varied in steps from 100 nsec to 50 μ sec, and the automatic scanning speed is selectable from 10 msec to 10⁵ sec full range. The number of samples averaged at any particular time in the scanning range can be selected by a proper combination

¹³ M. G. Badea and S. Georghiou, *Rev. Sci. Instrum.* **47**, 314 (1976).

¹⁴ J. W. Longworth, in "Creation and Detection of the Excited State" (A. A. Lamola, ed.) Vol. 1, Part A, p. 343. Dekker, New York, 1971.

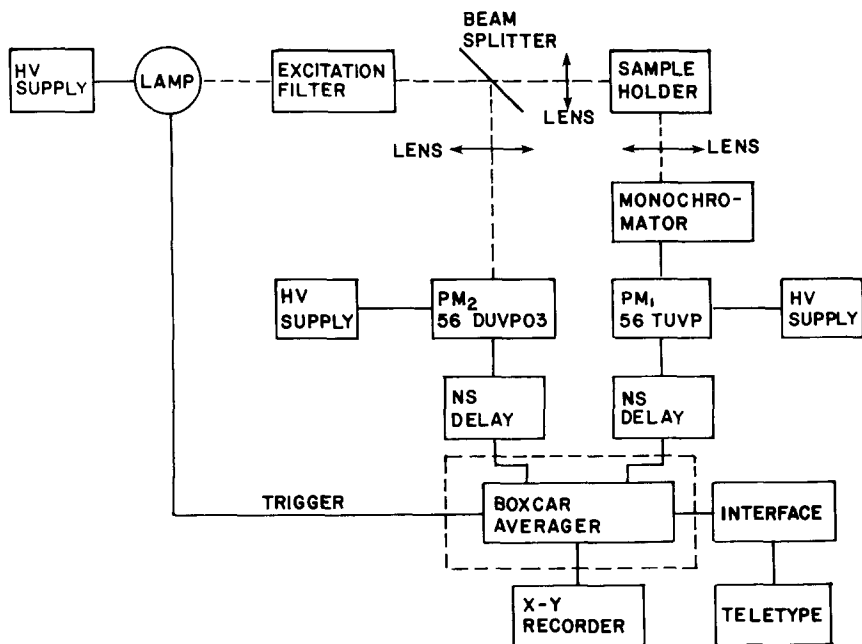


FIG. 4. Block diagram of a sampling fluorometer employing a boxcar averager. Details are given in the text.

of these two controls in relation to the repetition frequency of the signal to be measured.

Base line sampling, activated by a front panel switch, allows automatic correction for dc drifts. When the switch is activated, the averager samples and averages alternately the input signal and the base line for each gate opening. The output of the averager (for each gate opening) is then the difference between the two averaged samples. The time at which the base line is sampled, controlled by a front panel switch, is positioned well outside the time region of interest to avoid distortion of data. The output of the boxcar averager can be obtained either as a dc signal and/or in a digital format. It represents the time profiles of the excitation and the corresponding fluorescence decay over the previously selected scanning range. Subsequent data analysis can be performed on a suitable computer.

The principle of operation of this kind of instrumentation is identical with other pulse sampling scope instruments described in the literature by Steingraber and Berلمان,¹¹ Hundly *et al.*,¹⁵ and Hazan *et al.*¹⁶ In the latter

¹⁵ L. Hundley, T. Coburn, E. Gorwin, and L. Stryer, *Rev. Sci. Instrum.* **38**, 488 (1967).

¹⁶ G. Hazan, A. Grinvald, M. Maytal, and I. Z. Steinberg, *Rev. Sci. Instrum.* **54**, 1602 (1974).

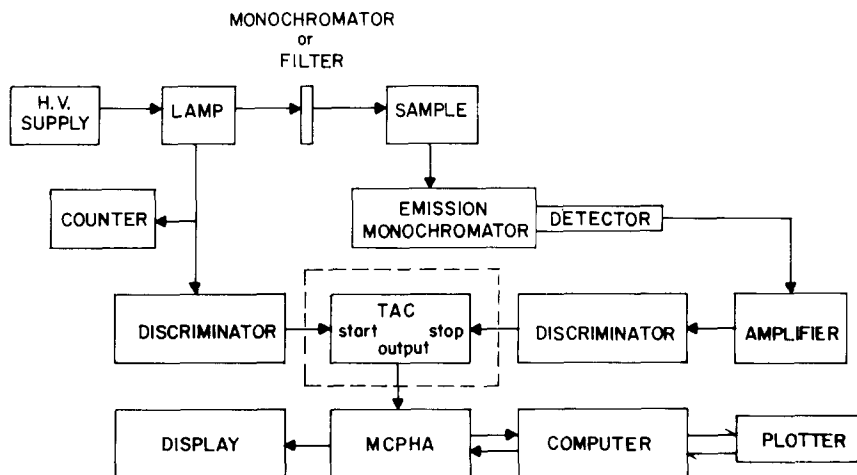


FIG. 5. Block diagram of a monophoton counting nanosecond decay fluorometer. Details are given in the text. MCPHA, multichannel pulse height analyzer.

a large number of sampling sweeps are averaged with the use of a mini-computer¹⁵ or a multichannel analyzer¹⁶ to eliminate the base line drifts and lamp intensity fluctuation. The P.A.R. boxcar averager can also be used in this mode of operation. Furthermore, its features of instantaneous ratio and base line sampling provide two additional capabilities for averaging the intensity fluctuations and the dc drifts. The performance characteristics of a particular fluorometer set-up employing a P.A.R. boxcar averager are described by Badea and Georghiou.¹³

ONE PHOTON PER EXCITING PULSE. The second method of detection used in pulse fluorometry is exemplified by instruments based on the monophoton counting procedure. This is an interval timing method. Instruments based on the monophoton counting method are available commercially^{17,18} and numerous variations and improvements have been described in the literature.¹⁹⁻²²

A schematic outline of a monophoton counting decay fluorometer is shown in Fig. 5. Light from the nanosecond flash lamp passes through an excitation filter or monochromator and is used to excite the sample. A po-

¹⁷ Ortec, Inc., Oak Ridge, Tennessee.

¹⁸ Photochemical Res. Assoc., Western Ontario, Canada.

¹⁹ R. Schuyler and I. Isenberg, *Rev. Sci. Instrum.* **42**, 813 (1971).

²⁰ W. R. Ware, in "Fluorescence Techniques in Cell Biology" (A. A. Thayer and M. Sernetz, eds.), p. 15. Springer-Verlag, Berlin and New York, 1973.

²¹ J. Yguerabide, in "Fluorescence Techniques in Cell Biology" (A. A. Thayer and M. Sernetz, eds.), p. 311. Springer-Verlag, Berlin and New York, 1973.

²² B. Leskovar, C. C. Lo, P. Hartig, and K. Sauer, *Rev. Sci. Instrum.* **47**, 1113 (1976).

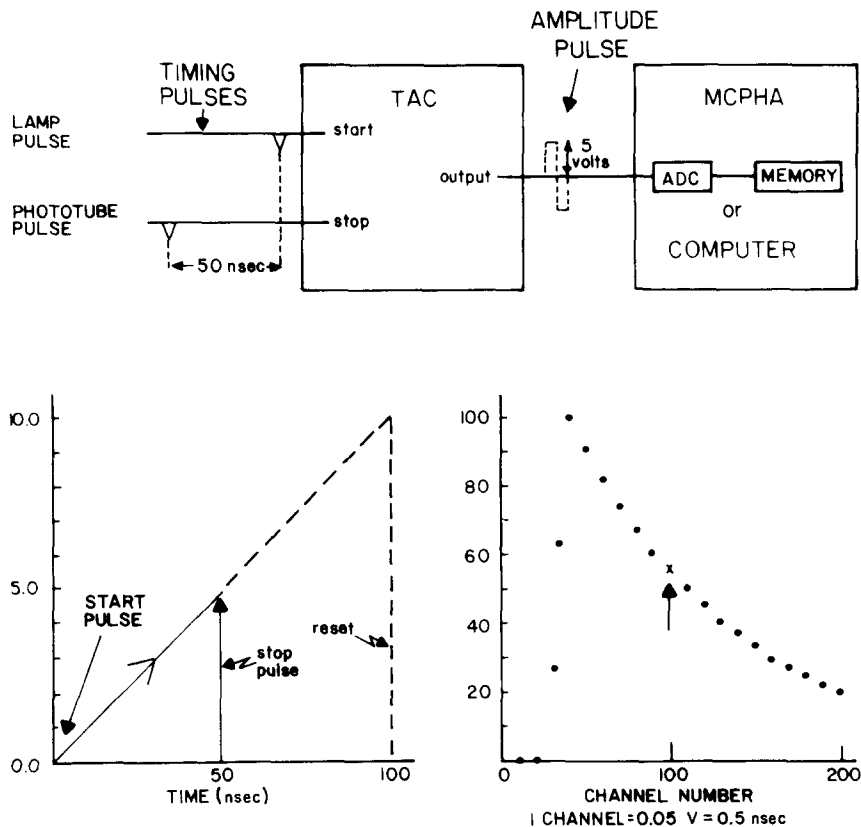


FIG. 6. Schematic illustration of the operation of a time to amplitude converter (TAC). A description is given in the text. ADC, analog to digital converter; MCPHA, Multichannel pulse height analyzer.

larizer may also be included in the light path. Fluorescence emission is usually observed at right angles to the excitation. The heart of a mono-photon counting instrument is the time to pulse height or time to amplitude converter (TAC). This is indicated in the dotted box in Fig. 5 and its function is shown in more detail in Fig. 6. This electronic device measures the time between the flash of the lamp and the arrival of a photon at the detector.

The start pulse for the TAC is obtained at the time of the lamp flash and initiates a voltage ramp linear with time on the nanosecond time scale. The start pulse has its origin either at an antenna placed near the spark gap or at a photomultiplier that directly views the lamp flash. The start pulses are shaped by a discriminator and counted before going to the TAC.

The voltage ramp is halted by a stop pulse. This signal has its origin at the photomultiplier which detects the photon emitted from the sample. The pulse is amplified and shaped by a discriminator before entering the TAC. This device now holds a signal whose amplitude is proportional to the time between the lamp flash and the photon emission. This information can be retained for several microseconds and then transferred through an analog to digital converter (ADC) to the memory of a multi-channel pulse height analyzer (MCPHA) or directly to a digital computer.

Typical operation of a TAC is illustrated in Fig. 6. The time between the lamp flash and a photomultiplier pulse is 50 nsec. This TAC gives a 10 V bipolar output pulse for 100 nsec. Thus in this case a 5 V pulse is passed through the ADC to the memory of the MPHA. A single count is added to the channel number proportional to the pulse amplitude (5 V in this case). The channel number is also proportional to the arrival time of the photon. In the present example, one channel equals 0.05 V which equals 0.5 nsec. The count is thus added to channel 100. The MPHA includes an oscilloscope display unit which gives a continuous display of counts versus channel number. This represents the fluorescence decay curve or if a scattering solution is placed in the sample compartment, the lamp flash time profile.

This procedure thus involves recording of a time interval and conversion to an analog signal followed by conversion of the analog signal back to digital form. Since only the first of these events must take place on the nanosecond time scale less demands for "fast electronics" exist than is the case with other pulse methods.

As will be described below, fluorescence decay data obtained by pulse methods is usually distorted by convolution with a nondelta pulse lamp profile. For this reason, it is necessary to obtain a lamp flash profile along with each decay curve. This is usually done by measuring the scatter of the lamp flash with a colloidal material such as Ludox.²³ The desired impulse response [$F(t)$] which describes the true kinetics of the fluorescence decay must then be extracted from the *experimental* convolved decay curve $R(t)$ (for *response* function) and $L(t)$ the experimental lamp flash profile.

If a timing drift occurs between the time that the lamp profile and the decay curve are obtained, adequate analysis of the data will be impossible. Hazan *et al.*¹⁶ described an alternative procedure for overcoming this problem. Collection of data is alternated between a cuvette containing a scattering suspension and a cuvette containing the fluorescence sample. In this way $R(t)$ and $L(t)$ are collected during the same time period and errors due to drift tend to average out. Easter *et al.*²⁴ use a similar

²³ Colloidal Silica, IBD-1019-69, trade name Ludox, Dupont, Wilmington, Delaware.

²⁴ J. H. Easter, R. P. DeToma, and L. Brand, *Biophys. J.* **16**, 571 (1976).

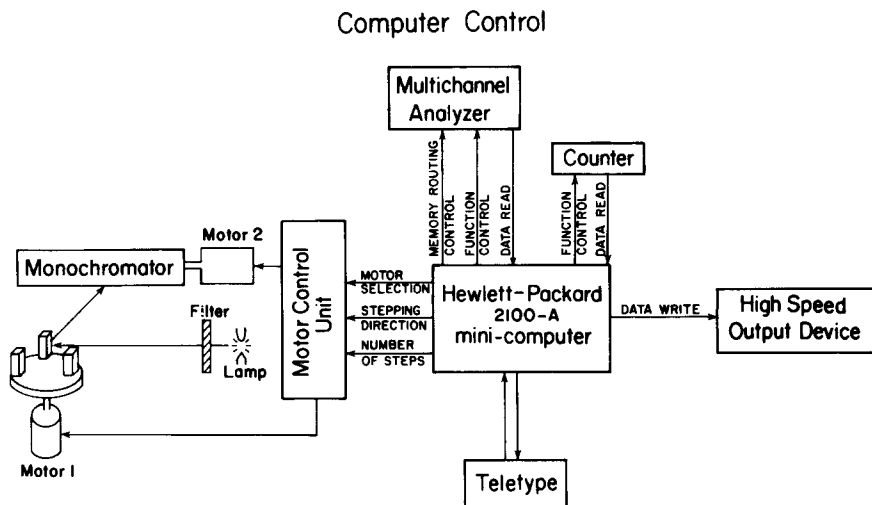


FIG. 7. Schematic diagram of the computer control over a monophoton counting decay fluorometer. The procedure used for the alternation of three samples is illustrated.

method which is shown in Fig. 7. Three cuvette holders are mounted on a turntable so that any one of three cuvettes can be positioned in the light path. This is accomplished by a stepper motor under control of a digital minicomputer. Light from a thyatron-gated flash lamp is focused on the sample with a lens and is passed through an interference filter to select the desired exciting wavelength. The cuvette turntable and the emission monochromator are driven by Slo-Syn stepper-motors models HS-50L which have 200 steps per 360° revolution. The motors are driven by Slo-Syn translators No. ST-1800BK. The translators are activated by a signal from a relay register in the minicomputer. Thus by means of the relay register output of the computer, a software program controls which motor is to be stepped (turntable or monochromator), the direction of the step, and the number of steps. Software control with the minicomputer thus enables the operator to alternate cuvettes with specified dwell times on each cuvette. Decay data can be collected at any desired emission wavelength.

Analysis of Fluorescence Decay

Procedures for data analysis are as important in nanosecond fluorometry as the instrumentation itself. This is particularly true in the case of pulse fluorometry. As was discussed above, the fluorescence is initiated by a short flash of light. The true fluorescence decay, $F(t)$ is the transient that follows excitation of the solution by a "delta" pulse i.e., an infinitely short pulse of light. $F(t)$, the true fluorescence decay, is also referred to as the impulse response. Since a delta pulse is infinitely narrow, excitation in

this way would precisely define the time origin from which the decay is to be measured. In practice most light pulses used for excitation have a finite width which does not allow a clear definition of the true time zero. The experimentally obtained fluorescence decay will be distorted by convolution with the lamp flash profile. This artifact is described by the convolution integral

$$R(t) = \int_0^t L(t')F(t - t') dt' \quad (5)$$

where $F(t)$ is the true fluorescence decay, $L(t)$ is the time profile of the excitation light pulse, and $R(t)$ is the response that will actually be obtained from the instrument followed by the light pulse $L(t)$. In a more qualitative sense the convolution integral can be described as the summation of the true fluorescence decays that would be obtained following excitation by an infinitesimal pulse of width Δt , centered about t_i . t_i covers in discrete steps the range of $L(t)$ the excitation profile. Each of these narrow pulses at t_i induces a fluorescence response at time t given by

$$R_i(t) = L(t_i) \Delta t F(t - t_i) \quad (6)$$

The argument $(t - t_i)$ expresses the fact that the time course of fluorescence decay is measured relative to the inducing excitation which is centered at time t_i .

In the absence of nonlinear optical effects the superposition of the infinitesimal responses up to time t gives the total fluorescence response. Thus

$$R(t) = \sum_{t_i=0}^{t=t} L(t_i) F(t - t_i) \Delta t \quad (7)$$

which becomes the convolution integral in the limit $\Delta t \rightarrow 0$:

$$R(t) = \int_0^t L(t')F(t - t') dt' \quad (8)$$

Here t' is a dummy variable of integration. Making the change of variables $t' = t - u$, we have

$$R(t) = \int_0^t L(t - u)F(u) du \quad (9)$$

Thus a nanosecond pulse fluorometer gives $R(t)$ and $L(t)$, and our task is to extract $F(u) \equiv F(t)$ the true impulse fluorescence response which may then be compared to theoretical predictions regarding kinetic mecha-

nisms. A large variety of numerical procedures have been devised and tested for carrying out this deconvolution procedure.²⁵⁻³⁰

It is convenient to divide these deconvolution procedures into two conceptual categories. First, those working in the real time domain, and, second, those working in a transformed domain. In the latter case, a linear operator is applied to the experimental data prior to performing the deconvolution.

Methods Working in the Real Time Domain. These are usually curve fitting techniques. They make use of a numerical convolution rather than a deconvolution procedure. A physically plausible analytical expression for the impulse response is assumed. In most cases a sum of exponential terms is assumed for $F(t)$:

$$F(t) = \sum_{i=1}^n \alpha_i e^{-t/\tau_i} \quad (10)$$

Thus the fluorescence decay is defined in terms of several decay constants, τ_i , and a set of amplitudes or preexponential terms α_i . In the fitting procedure suitable guesses are selected for the α_i 's and τ_i 's, and $F(t)$ is then numerically convoluted with the experimental $L(t)$. The theoretical $R(t)$ thus obtained is compared with the experimental $R(t)$. The free parameters in $F(t)$ are then adjusted until the best fit between the calculated and experimental $R(t)$ is obtained. Ware *et al.*²⁶ have described the use of a linear least squares procedure. In this method the decay times are set constant and the equations are solved for the best values of the preexponential terms. Grinvald and Steinberg^{27,31} have used the nonlinear least squares method of Marquardt (see Bevington³²) to solve for both the decay constants and amplitudes describing fluorescence decay data. This technique has also been found to be valuable in our own laboratory.²⁴

The Marquardt algorithm of nonlinear least squares employs a dual search along the χ^2 hypersurface defined by

$$\chi^2 = \sum_{i=1}^n W_i [R(t)^{\text{expt}} - R(t)^{\text{calc}}]^2 \quad (11)$$

²⁵ I. Isenberg, R. D. Dyson, and R. Hanson, *Biophys. J.* **13**, 1090 (1973).

²⁶ W. Ware, L. J. Doemeny, and T. L. Nemzek, *J. Phys. Chem.* **77**, 2038 (1973).

²⁷ A. Grinvald and I. Z. Steinberg, *Anal. Biochem.* **59**, 583 (1974).

²⁸ A. Gafni, R. L. Modlin, and L. Brand, *Biophys. J.* **15**, 263 (1975).

²⁹ B. Valeur and J. Moirez, *J. Chim. Phys. Phys. Chim. Biol.* **70**, 500 (1973).

³⁰ J. N. Demas and A. W. Adamson, *J. Phys. Chem.* **75**, 2463 (1971).

³¹ A. Grinvald, *Anal. Biochem.* **75**, 260 (1976).

³² P. R. Bevington, "Data Reduction and Error Analysis for the Physical Sciences." McGraw-Hill, New York, 1969.

for a minimal value of χ^2 . χ^2 is considered as a function of the parameter increments that are defined with respect to initial parameter guesses α_i^0 and τ_i^0 , which must be specified at the start of each search. There are two searching paths, one for parameter guesses which establish χ^2 far removed from the minimum and the other for χ^2 values near the minimum. The two searching paths are apportioned automatically within the algorithm. ω_i is a statistical weighting factor defined by the principles of least squares and for the case of photon counting error may be approximated by

$$\omega_i = 1/R(t) \quad (12)$$

Grinvald and Steinberg²⁷ have emphasized the importance of using correct weighting factors in least squares analysis.

In our own laboratory, we have found it valuable to carry out the non-linear least squares analyses with an interactive computer. Following Grinvald and Steinberg,²⁷ the "goodness of fit" is judged by (a) visual inspection of the superimposed $R(t)^{\text{calc}}$ and $R(t)^{\text{expt}}$. It is especially useful to inspect the rise and fall of the decay curves; (b) evaluation of χ^2 ; (c)

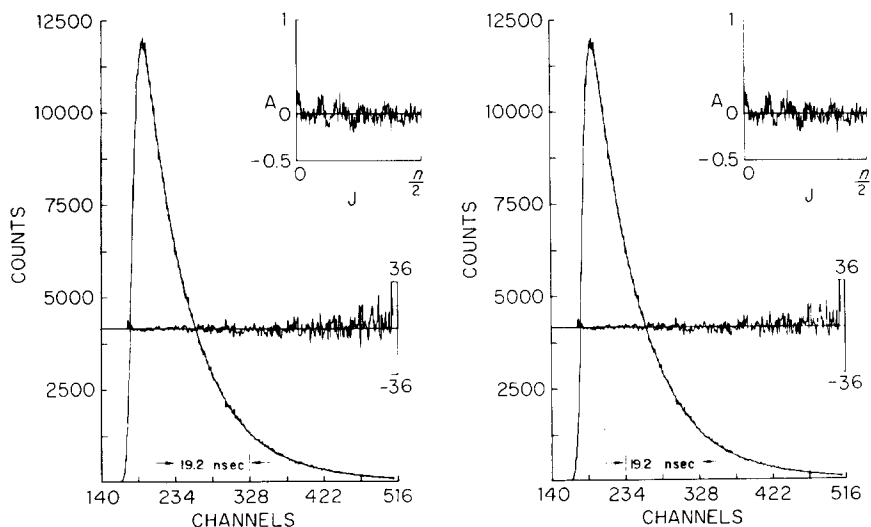


FIG. 8. Fluorescence decay of 9-cyanoanthracene in ethanol. This type of plot aids in determining the "goodness of fit" of fluorescence decay data. Shown are the experimental decay curve, the best theoretical data convolved with the lamp flash. The residuals between the theoretical and experimental decay curves are shown in the center and the autocorrelation of the residuals are shown in the inset at the upper right. The results of an analysis in terms of a single exponential decay law are shown on the left. A decay time of 11.8 nsec was obtained. An analysis in terms of a double exponential decay law is shown on the right.

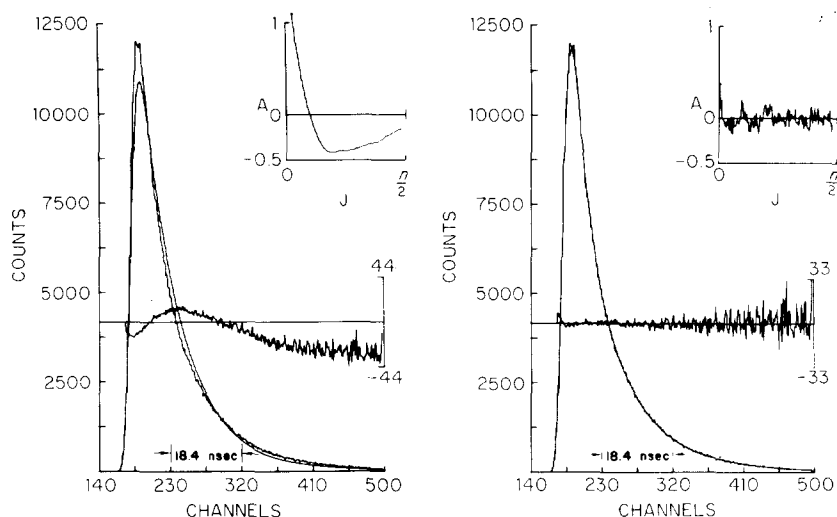


FIG. 9. Fluorescence decay of an equimolar mixture of anthracene ($\tau = 4.2$ nsec) and 9-cyanoanthracene ($\tau = 11.8$ nsec) in ethanol. The meaning of different portions of the figure is similar to that indicated in the legend to Fig. 8. The best fit to a single exponential decay law is shown on the left. The right shows the fit to a double exponential decay law. Decay times of 4.2 nsec and 11.8 nsec were obtained.

evaluation of the residual [$R^{\text{calc}}(t) - R^{\text{expt}}(t)$]; and (d) evaluation of the autocorrelation function of the residuals.

Typical results of an analysis of data showing both single and double exponential decay behavior are shown in Figs. 8 and 9. Figure 8 shows the experimental fluorescence decay, $R(t)^{\text{expt}}$ of 9-cyanoanthracene dissolved in ethanol. The vertical axis indicates the number of counts accumulated and the X axis is in channels since time zero is ill-defined in convolved data. There are 0.2 nsec/channel. Figure 8 (left) the best fit $R(t)^{\text{calc}}$ for a single exponential decay law superimposed on the experimental. The residuals between the theoretical and experimental data are shown in the center of the figure and the autocorrelation function of the residuals is shown in the inset at the upper right. The use of the autocorrelation function to betray a nonrandom distribution of the residuals was introduced for fluorescence decay data by Grinvald and Steinberg.²⁷ Figure 8 (right) shows the same data with an analysis in terms of a double exponential decay law. There is little or no improvement in any of the criteria for a good fit. This data is thus in accord with a single exponential decay law with a decay time of 11.8 nsec.

Figure 9 (left) shows the results of an analysis of the fluorescence decay of a mixture of 9-cyanoanthracene and anthracene in ethanol. In this case the best fit in terms of a single exponential decay law is clearly

inadequate. The experimental and theoretical $R(t)$ show significant deviations. This systematic deviation is quite apparent in the residuals whose nonrandomness is indicated by the autocorrelation function. In contrast, Fig. 9 (right) indicates that a double exponential decay law is adequate to give a good fit to $R(t)$. Grinvald and Steinberg²⁷ have emphasized the use of standard compounds which show single exponential decay behavior to uncover systematic errors in nanosecond decay fluorimeters. We also recommend their use in this way. The "real time" search methods are in actuality not procedures for deconvolution but rather iterative convolution methods.

Methods Making Use of Transformed Domains. In these numerical procedures the measured lamp flash $L(t)$ and the fluorescence response $R(t)$ are transformed to another domain by the application of a linear operator prior to further computations. The transformation can be carried out with operators that assume an infinite range for the time domain as is the case with the Laplace,^{28,33} Fourier³⁴ and moment³⁵⁻³⁹ operators. Alternatively, the transformation can assume a finite time range as is the case with the method of modulating functions²⁹ and the phase plane technique.³⁰

There is an important difference between these two classes of transformations. Methods employing operators of the first class must contend with the difficulties imposed by the assumed infinite time range as compared with the finite time range over which experimental data is obtained. This problem does not exist with the second type of transformations.

Several of the transformation techniques aim at reducing the convolution integral to a system of simultaneous algebraic equations which are solved for the decay parameters appearing in the analytical expression for the fluorescence decay law.

As an example of the first class of transformations, the procedure for analysis of fluorescence decay curves by means of the *Laplace method*^{28,32} will be described.

The convolution theorem states that if functions are related by a *convolution* product in the time domain, they will be related by a simple *algebraic* product in the Laplace domain. The basic computational procedure is as follows: The algorithm computes the Laplace transform of $L(t)$ and $R(t)$ and determines their ratio. This gives the Laplace transform of the

³³ W. P. Helman, *Int. J. Radiat. Phys. Chem.* **3**, 283 (1971).

³⁴ S. W. Provencher, *Biophys. J.* **16**, 27 (1976).

³⁵ I. Isenberg and R. D. Dyson, *Biophys. J.* **9**, 1337 (1969).

³⁶ I. Isenberg in "Biochemical Fluorescence Concepts" (R. Chen and H. Edelhoch, eds.), Vol. I, p. 43. Dekker, New York, 1975.

³⁷ I. Isenberg, *J. Chem. Phys.* **59**, 5696 (1973).

³⁸ I. Isenberg, *J. Chem. Phys.* **59**, 5708 (1973).

³⁹ Z. Bay, V. P. Henri and H. Kanner, *Phys. Rev.* **100**, 1197 (1955).

impulse response. Conversion from Laplace space to real time presents some numerical difficulties. Instead, the numerical Laplace of the impulse response is set equal to the Laplace transform of the analytical expression for the impulse response.

The Laplace transform $M(s)$ of a function $M(t)$ is defined:

$$M(s) = L[M(t)] = \int_0^{\infty} M(t) e^{-St} dt \quad (S \geq 0) \quad (13)$$

By applying the Laplace operator to the convolution integral, we obtain

$$\begin{aligned} L[R(t)] &= L\left(\int_0^t L(t') F(t-t') dt'\right) \\ R(S) &= L(S) F(S) \end{aligned} \quad (14)$$

Thus the true fluorescence decay in Laplace space is obtained by simply dividing the transforms of the response to that of the exciting pulse.

If the assumed decay law is a sum of exponential terms, it is easily shown that

$$L[F(t)] = L\left(\sum_{i=1}^n \alpha_i e^{-t/\tau_i}\right) = \sum_{i=1}^n \frac{\alpha_i}{S + 1/\tau_i} \quad (15)$$

S is the exponent in the Laplace transform defined by Eq. 13. Thus,

$$F(S) = \frac{L(S)}{R(S)} = \sum_{i=1}^n \frac{\alpha_i}{S + 1/\tau_i} \quad (16)$$

A computer is used to evaluate $F(S)/L(S)$ for $2n$ values of S . A set of $2n$ simultaneous equations is obtained and solved for the n amplitudes and n decay constants. Procedures dealing with the finite limit of the data (the cutoff correction) and the choice of S value have been described²⁸ and will not be covered in detail here.

It must be emphasized that while the distortion in the fluorescence decay introduced by the finite width of the lamp flash is eliminated by the deconvolution procedure, if *actual* scattered light passes through the optics and contributes to the decay signal, it must be subtracted prior to analysis. As an alternative option a scatter term may be included in the Laplace algorithm. In the case of decay data which contains scattered light, the Laplace transform of the decay becomes

$$F(S) = L(S) R(S) + C L(S) \quad (17)$$

with C being the relative contribution by scattered light. In this case, $2n + 1$ Laplace transforms must be computed, and $2n + 1$ simultaneous

equations must be solved. The reliability of the numerical method decreases the more simultaneous equations there are. It is thus always desirable to measure the scatter contribution in an independent experiment and subtract it from $R(t)$ before analysis.

The *method of moments* belongs to the same class of techniques as the Laplace approach. It has been used for analyses of decay data for many years.^{39,40} Isenberg has explored the application of this method to fluorescence decay studies.³⁴⁻³⁷ He has investigated the statistics involved in these analyses and has shown that a contribution due to scattered light can be taken into account.

Since the method of moments was described in a previous article in this series,⁴¹ it will not be described in detail here. Briefly, the approach is quite similar to that taken in the Laplace method.

The K th moment transform of a function $F(u)$ is defined as

$$M^K[F(U)] = \int_0^\infty U^K F(U) dU \quad (18)$$

By applying the moment operator on both sides of the convolution integral the convolution product is transformed into a linear combination of moment transforms. Thus, we have

$$R(t) = \int_0^t L(t-t')F(t') dt' \quad (19)$$

$$\begin{aligned} M^K[R(t)] &= M^K \left(\int_0^t L(t-t')F(t') dt' \right) \\ &= \int_0^t M^K[L(t-t')]F(t') dt' \end{aligned} \quad (20)$$

The last equality is possible due to the linear property of the moment operator. It can be shown that if the fluorescence decay [impulse response = $F(t)$] is represented as a sum of exponentials, the integral is equivalent to the following algebraic relation:

$$\frac{M^K[R(t)]}{1} = \sum_{s=1}^{K+1} G_s \frac{M^{(K+s-1)}[E(t)]}{(K+l-s)!} \quad (21)$$

where G_s is combination of the assumed parameters for $F(t)$ given by

$$G_s = \sum_{n=1}^N \alpha_n \tau_n^{-1} \quad (22)$$

The linear set of algebraic equations obtained for different values of K can be solved for G_s 's. A set of $2N$ G_s 's completely characterizes a given

⁴⁰ Ph. Wahl and H. Lami, *Biochim. Biophys. Acta* **133**, 233 (1967).

⁴¹ J. Yguerabide, Vol. 26, Part C, p. 498.

set of assumed decay parameters. In particular, the parameters could be extracted from the set $G_{d+1}, G_{d+2}, \dots, G_{d+2N}$ where d , a positive integer, is called the order of moment index displacement.³⁶ Usually the set with $d = 0$ or $d = 1$ is used. The advantage of using the set with $d = 1$ is that it enables to correct for a variety of systematic instrumental errors like the time shifts and scattered light either completely or in a perturbation sense. It has been shown⁴² that this moment index displacement of order one can completely correct for scattered light having a different wavelength than that of fluorescence, whereas it can correct only in a perturbation sense, i.e., to minimize an already small effect if the scattered light has the same wavelength as the fluorescence or if a time origin discrepancy exists between the measured curves $R(t)$ and $L(t)$ (zero time shift error). Moment index displacement will also reduce errors due to slow lamp drift during collection of an individual curve. The drawback of going to higher moments is that the collection time will have to be increased in order to calculate them with a satisfactory accuracy. This will increase errors associated with long-term time drifts.

As is the case with the Laplace method, the algebraic relations obtained by applying the moment operator to the convolution integral are theoretically valid only if the time range is infinite. As the real data is always collected over a finite range, a cut-off procedure has been devised which by iteration yields a self-consistent set of parameters. It has been found useful to exponentially depress the raw data prior to analysis in order to reduce the number of iterations and improve the convergence. This is always possible because the convolution integral is invariant to the multiplication by a time exponential.

The problems associated with the iterative convergence are not present when an operator which does not assume an infinite time range for data acquisition is used in the transformation. As an example of this second class operators the *method of modulating functions* will be described in some detail. This method first proposed by Loeb and Cahen⁴³ for the determination of unknown coefficients of linear differential equations has been introduced to the fluorescence field by Valeur and Moirez.²⁹ The authors observed that by assuming a sum of exponentials for the fluorescence decay the convolution integral can be put in the following differential form:

$$R + \alpha_1 \dot{R} + \alpha_2 \ddot{R} + \dots + \alpha_N R^{(N)} = \beta_1 L + \beta_2 \dot{L} + \dots + \beta_N L^{(N)} \quad (23)$$

where (N) stands for the N th derivative with respect to time, α_i is a set of constant coefficients dependent only on the lifetimes, and β_i is a similar set depending both on the lifetimes and amplitudes.

⁴² E. Small and I. Isenberg, *Biopolymers* **15**, 1093 (1976).

⁴³ J. Loeb and G. Cahen, *Automatisme* **8**, 479 (1963); *IEEE Trans. Autom. Control* **ac-10**, 359 (1965).

The method aims at eliminating the first and all higher-order time derivatives of both $R(t)$ and $L(t)$ from Eq. (23) by multiplying it with a set of "modulating functions" followed by integration by parts. The "modulating functions" are the set of functions which together with their time derivatives to the N th order are zero at the limits of the collection time range $(0, T)$. With $\rho(t)$ representing any such function Eq. (23) becomes

$$\begin{aligned} \alpha_1 \int_0^T R \dot{\rho} dt - \alpha_2 \int_0^T R \ddot{\rho} dt + \cdots \cdots (-1)^{N-1} \alpha_N \int_0^T R \rho^{(N)} dt \\ + \beta_1 \int_0^T L \rho dt - \beta_2 \int_0^T L \dot{\rho} dt \\ + \cdots \cdots (-1)^{N-1} \beta_N \int_0^T L \rho^{(N-1)} dt = - \int_0^T R \rho dt \end{aligned}$$

Thus the time derivatives of $R(t)$ and $L(t)$ have been replaced by the time derivatives of an *analytical* function $\rho(t)$. By using $2N$ such "modulating function" a system of $2N$ linear equations is obtained from which α_i and β_i are obtained. From the set α_i the lifetimes are extracted and their values introduced in the set β_i to obtain the amplitudes. It is important to note that the integration has been performed only from 0 to T the range in which both $L(t)$ and $R(t)$ were numerically defined. There is, in principle, no error due to truncation.

The gist of the method consists of efficiently "modulating" the shape of the experimental curves $R(t)$ and $L(t)$. Therefore the choice of the "modulating functions" is somewhat dependent on the shape of the experimental curves. Valeur and Moirez used functions of the type $\rho(t) = t^n(T-t)^p$ for which the exponents n and p were arbitrary, but greater than $N-1$. For further details regarding their choice and the use of the alternate method of truncated moments for the calculation of the amplitudes the reader is referred to the original paper.²⁹

Comparison of Deconvolution Techniques. McKinnon *et al.*⁴⁴ have carried out a detailed evaluation of the various procedures for deconvolution of fluorescence decay data. They found that the iterative convolution procedure gave good recovery of decay parameters under a variety of conditions. The reader is referred to the original paper which includes an excellent discussion of the problems associated with the analysis of fluorescence decay data.

Time-Resolved Emission Spectra

Nanosecond time-resolved emission spectra (TRES) are fluorescence spectra obtained at discrete times during the fluorescence decay. For example with reference to the decay curve shown in Fig. 10, fluorescence emission spectra might be obtained during the time window indicated by

⁴⁴ A. E. McKinnon, A. G. Szabo and D. R. Miller, *J. Phys. Chem.* **81**, 1564 (1977).

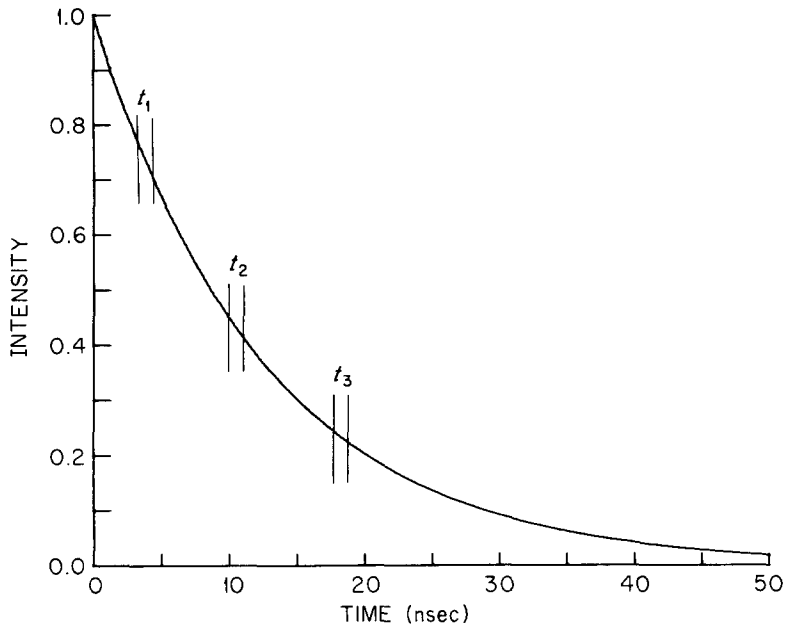


FIG. 10. Fluorescence decay curve with individual time windows.

t_1 or t_2 or t . These spectra will be defined in terms of both *spectral* and *time* resolution. The complete data matrix available may be described by a three dimensional surface $I(\lambda, t)$, representing the fluorescence intensity at all wavelengths and times during the fluorescence decay. Figure 11 shows an example of such a surface. It represents the decay of 2,6-toluidinonaphthalene (2,6-TNS) adsorbed to egg lecithin vesicles. In this case, there is a shift of the fluorescence emission to lower energies as a function of decay time. This phenomenon has been attributed to excited state solvation interactions.⁴⁵ Nanosecond time-dependent spectral shifts have been investigated by Ware,^{46,47} Egawa *et al.*,⁴⁸ and others. Spectral shifts of this type have been observed with fluorophores bound to proteins^{49,50} and adsorbed to phospholipid vesicles.⁵¹⁻⁵³ Apparent nanosec-

⁴⁵ J. H. Easter, R. P. DeToma, and L. Brand, *Biophys. J.* **16**, 571 (1976).

⁴⁶ W. R. Ware, P. Chow, and S. K. Lee, *Chem. Phys. Lett.* **2**, 356 (1968).

⁴⁷ W. R. Ware, S. K. Lee, G. J. Brant, and P. P. Chow, *J. Chem. Phys.* **54**, 4729 (1971).

⁴⁸ K. Egawa, N. Nakashima, N. Mataga, and C. Yamanaka, *Bull. Chem. Soc. Jpn.* **44**, 3287 (1971).

⁴⁹ A. Gafni, R. P. DeToma, R. E. Manrow, and L. Brand, *Biophys. J.* **17**, 155 (1977).

⁵⁰ L. Brand and J. R. Gohlke, *J. Biol. Chem.* **246**, 2317 (1971).

⁵¹ R. P. DeToma, J. H. Easter, and L. Brand, *J. Am. Chem. Soc.* **98**, 5001 (1976).

⁵² J. H. Easter, R. P. DeToma, and L. Brand, *Biochim. Biophys. Acta* **508**, 27 (1978).

⁵³ M. G. Badea, R. P. DeToma, and L. Brand, in "Biophysical Discussions: Fast Biochemical Reactions in Solutions, Membranes, and Cells" (V. A. Parsegian, ed.). The Rockefeller Univ. Press, Airlie House, Virginia, 1978.

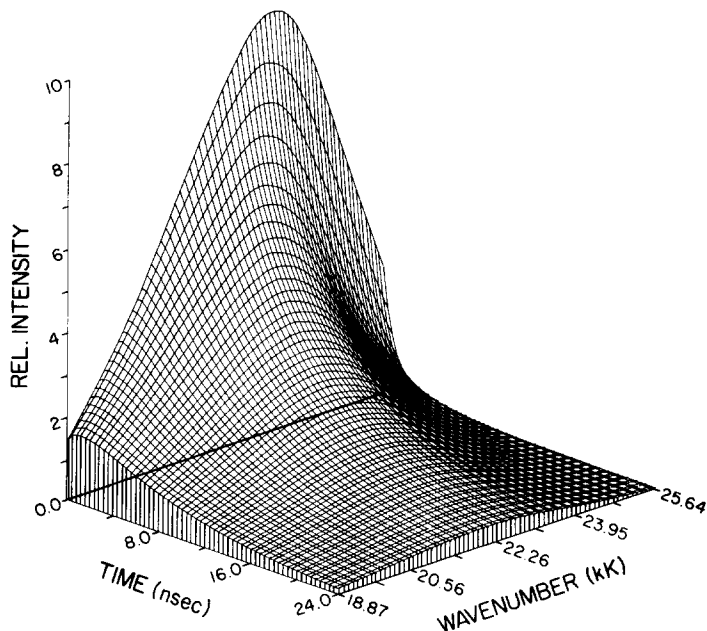


FIG. 11. Three-dimensional representation of the fluorescence intensity as a function of time and energy. This is for 2,6-*p*-toluidinonaphthalene (11 mM) adsorbed to egg L- α -lecithin vesicles (0.86 mM in lecithin) at 7°.

ond time-dependent spectral shifts may have their origin either in ground state heterogeneity or in excited state interactions. Both situations are of interest in biochemistry. While it is of interest to examine fluorescence decay curves as a function of emission wavelength, additional information can be obtained from the TRES.

Nanosecond pulse fluorimeters can easily be used to generate time resolved emission spectra. Either of two instrumental approaches can be used. In the first, a "window" is set for a particular time after the lamp flash and with a desired time width. The light signal is scanned with an emission monochromator and time resolved spectra are directly produced. This can be done with either a sampling instrument or with a monophoton counting instrument. Thus, with reference to Figs. 5 and 6, a single channel analyzer (SCA) is inserted into the system between the TAC and the MCPHA. This electronic device (SCA) can be set to allow a pulse to pass only if it is within some specified voltage limits. Thus, in the example shown in Fig. 6 the SCA might be set to pass a pulse only if it has a voltage between 4.95 and 5.05 V. Since 0.05 V equals 0.5 nsec, the "time window" in this case would be 1 nsec. The MCPHA is used in a multichannel scaling (MCS) mode in this case. Channels are addressed sequentially in phase with the movement of the emission monochromator.

Each channel now represents a wavelength and the appropriate setting of the single analyzer enables one to obtain a TRES with the desired time and spectral resolution.

The major drawback to a procedure of this type is that the time resolved emission spectra obtained will be distorted by convolution errors.⁴⁵ In addition time-zero is ill defined. While there is no way of correcting for convolution artifacts when time resolved spectra are obtained as described above, an alternative procedure is available which will be described below.

The windowing technique with the use of a SCA as described above also has applications of value in steady-state fluorescence instrumentation. For example it can be used to reduce errors due to light scattering in fluorescence emission spectroscopy. Once again the MCPHA is used in the MCS mode. In our laboratory we adjust the scaling speed and the monochromator to give 1 nm/channel. The window on the SCA is now set to eliminate pulses arriving during the first 2 nsec after the flash but to pass all later pulses. Thus photons originating in Rayleigh scattering are eliminated while delayed fluorescence photons are recorded. As an example, Fig. 12 shows the fluorescence emission spectrum of 9-

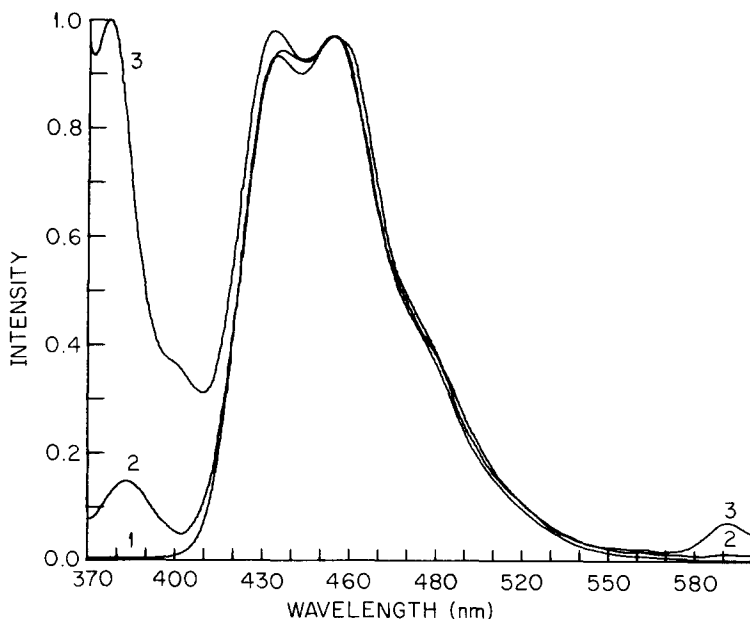


FIG. 12. Fluorescence emission spectra of 9-aminoacridine obtained by photon counting. (1) 9-Aminoacridine in water; (2) identical to (3), except the single channel analyzer is set so as to eliminate photons arriving within 3 nsec after the lamp flash; (3) 9-aminoacridine and Ludox to give rise to scattered light.

aminoacridine obtained under conditions of rather poor spectral resolution. Excitation was with a nitrogen flash lamp (see Fig. 1 for spectral emission) without the use of an excitation filter or monochromator. Ludox was included in the cuvette to enhance light scattering. Indeed a very significant scatter band is seen between 360 and 410 nm, and there is even a significant distortion at the main emission band of the fluorophore. The second-order scatter bands make a very significant contribution above 540 nm where the fluorescence intensity is low. When the time window is set to pass only photons arriving after 2–3 nsec, the scatter contribution is greatly reduced. The technique of time resolution can also be used to accentuate the contribution due to emission from one of a pair of fluorophores in a mixture. This assumes the two fluorophores have different decay times. This approach may also have value in Raman spectroscopy where errors due to contribution by fluorescence to the scatter may be significant.

It was indicated above that TRES obtained by the SCA method are distorted by convolution errors. As an alternative procedure for obtaining TRES, fluorescence decay curves are obtained at wavelength intervals over the spectral region of interest. This data is then deconvolved by the procedures already described.

Since a large number of decay curves must be obtained, these experiments are conveniently carried out under computer control as shown in Fig. 7. Lamp flash profiles and decay curves are collected making use of the alternation technique already described.

With reference to Fig. 7, the sequence of computer directives during the course of an experiment can be divided into three phases: collection, search, and output. In the collection phase the cuvette turntable is positioned with the fluorescence sample in the optical path, the monochromator is set to a previously specified wavelength, the MCPHA is started in the accumulation mode, and totalization of lamp flashes with the counter is initiated. After a designated decay dwell time (typically 5 to 15 min) data collection is stopped and the information in the MCPHA and the counter is transferred to computer memory. The cuvette turntable is then positioned so that a scattering is in the optical path, the emission monochromator is set to the exciting wavelength and data collection is initiated. After the specified collection time for the lamp profile, accumulation is stopped and the data is transferred to computer memory. In phase two of the computer operation the data representing the decay and the lamp flash are searched to determine whether specified peak and/or total counts have been obtained. If data collection is not complete, control is returned to the first phase of operation. When data collection is complete, the decay curve and the lamp profile are transferred to the output device

(a disc, magnetic tape, or paper tape) together with the wavelengths, curve index number, peak counts, and counter monitor. The computer then initiates collection of the data for the next wavelength. The entire decay data matrix required for a TRES is now available.

As a first step each decay curve is deconvolved using the method of nonlinear least squares as an empirical deconvolution procedure. A sum of up to five exponential terms is usually sufficient to give a good empirical fit to any fluorescence decay curve. In this way reliable impulse response decay curves $F(t)$ are produced in spite of the fact that the α 's and τ 's obtained may or may not have direct physical meaning. It has been found with the use of computer simulation that nonlinear least squares with a multiexponential fitting function provides a powerful deconvolution method for fluorescence decay data.⁴⁵

The impulse response curves $F(\lambda, t)$ are normalized to a steady-state emission spectrum obtained on the same instrument. The computer now contains the data matrix required to generate the time resolved spectra at any time t . The logical sequence of computer operations in constructing a TRES is shown in Fig. 13. Figure 13A indicates convolved decay curves obtained at three representative wavelengths. These curves have been collected to about the same number of counts at the peak. Figure 13B shows the same data deconvolved by the method of nonlinear least squares. Figure 13C shows that the three decay curves have been normalized to the corrected steady-state emission spectrum obtained using the same instrument. It is worth mentioning that in this example the initial rise seen in $F(t)$ at the longest wavelength provides evidence that an excited state reaction is taking place. Figure 13D shows TRES generated at the three times (0.5, 2, and 11 nsec) indicated by the arrows in Fig. 13C. A numerical derivative procedure can now be used to find the maximum of the decay at any time and the system can be characterized by a plot of $I_{\max}(t)$. These curves can in turn be analyzed in terms of a multiexponential decay law.

Time-Resolved Emission Anisotropy

Fluorescence emitted by a sample is usually found to be polarized at least at early time during the fluorescence decay. This phenomenon can be understood in terms of the existence of fixed preferential directions **a** and **e** in the molecule along whose directions the transition moments for absorption and emission of light acquire their *maximum* value. Fluorescence polarization is observed even if the sample consists of a random distribution of fluorophores. This is because the processes of absorption and emission by individual molecules are always anisotropic. Thus the

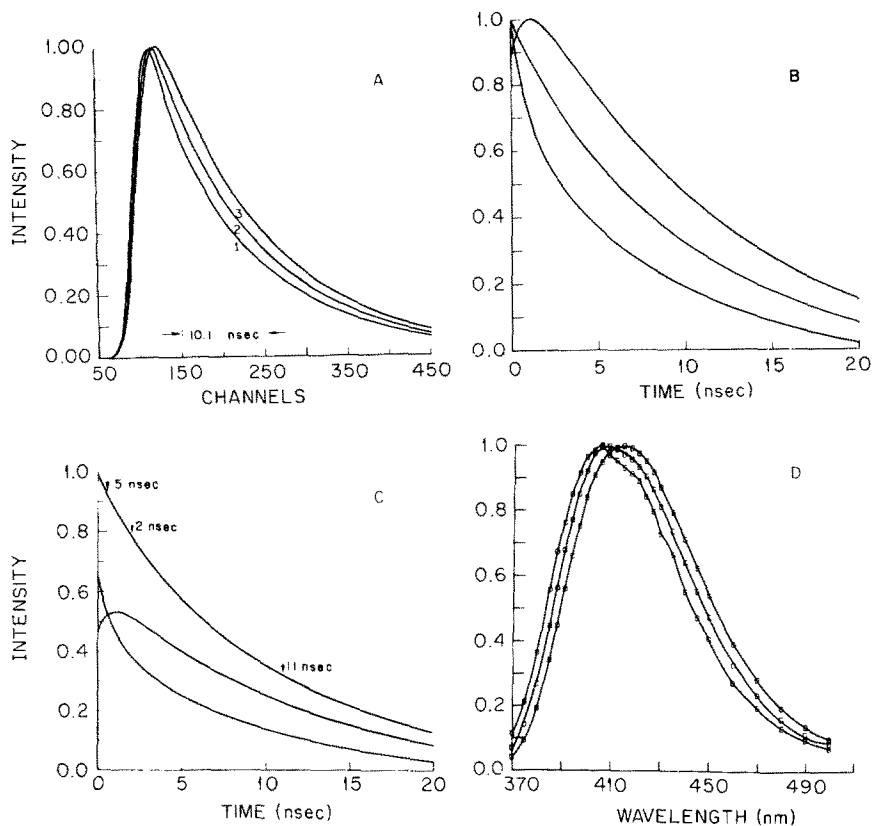


FIG. 13. Illustration of the sequence of computer operations used to generate deconvolved TRES. 2-Anilino-naphthalene ($1 \mu\text{M}$) in DML (dimyristoglycerol) vesicles. The lipid to dye ratio was about 700. The temperature was 37° . Excitation was at 315 nm and the emission wavelength was (1) 394, (2) 409 and (3) 445 nm. (A) shows the convolved decay curves collected to constant peak height. (B) shows the decay curves scaled according to the steady-state spectra. (C) shows the decay curves deconvolved to obtain the impulse response curves. (D) the intensity obtained from the impulse response at a particular time plotted against wavelength. The deconvolved TRES are normalized at the peak.

probability of absorption of polarized light having the electric vector \mathbf{E} is proportional to the square of its component along the direction \mathbf{a} . The emission from an individual fluorophore is always polarized with the electric vector in a plane defined by \mathbf{e} and the direction of detection. Fluorescence polarization from a sample is observed even if the excitation is performed with unpolarized (natural) light. This is explained by the fact that light by its nature is anisotropic, since the possible orientations of the exciting electric vector \mathbf{E} are always confined in a plane perpendicular to the direction of propagation. The simple model of linear dipole oscillators

is based on the quantum mechanical picture of electric dipole transitions and is valid only in the limit of strict monochromaticity. It has been able to explain, however, at least in a phenomenological sense, all the known facts about polarization of broad band luminescence.

The interaction of light with a random array of anisotropic fluorophores results in the photoselection of an anisotropic ensemble of excited molecules from the original isotropic system. This photo-selected subensemble will have a nonrandom mutual orientation of their absorption and emission dipoles. The anisotropic distribution will be reflected macroscopically by a measurable polarization. Any process that reduces this nonrandomness will have a depolarizing effect.

Polarized light exhibits a variation in its intensity, when viewed through a polarizer whose transmission axis orientation in space is changed. Let us call v (vertical) the direction perpendicular to the plane of excitation detection and H (horizontal) any direction in this plane perpendicular to either the line of excitation or detection (as the case may be). The fluorescence polarization depends on the polarization of the exciting light and on the angle between direction of excitation and detection.

The parameters usually used to quantitate this dependence are the polarization (p) introduced by Perrin⁵⁴ and the emission anisotropy (r) introduced by Jablonski.⁵⁵ In time-dependent notation, they are defined by

$$p(t) = \frac{I_V(t) - I_H(t)}{I_V(t) + I_H(t)} = \frac{D(t)}{I_V(t) + I_H(t)} \quad (24)$$

and

$$r(t) = \frac{I_V(t) - I_H(t)}{I(t)} = \frac{D(t)}{S(t)} \quad (25)$$

where $I_V(t)$ and $I_H(t)$ are the fluorescence intensities detected through a polarizer whose transmission axis is aligned perpendicular and parallel to the excitation detection plane, respectively; $I(t)$ is a locally defined measure of the total emission intensity also called the sum function $S(t)$ and $D(t)$ is the difference function. Because it is defined in terms of the total emission, $r(t)$ has been found more convenient in theoretical calculations and is nowadays used preferentially. For later reference some of the expressions for $r(t)$ and the corresponding relationships for $p(t)$ are given below. For the usual 90° geometry of excitation detection we have the following.⁵⁶

For linearly polarized excitation with $\mathbf{E} \parallel \mathbf{V}$

⁵⁴ F. Perrin, *J. Phys. Radium* [6] 7, 390 (1926).

⁵⁵ A. Jablonski, *Acta Physiol. Pol.* 16, 471 (1957).

⁵⁶ A. Jablonski, *Bull. Acad. Pol. Sci., Ser. Sci. Math., Astron. Phys.* 8, 259 (1960).

$$r(t) = \frac{I_V(t) - I_H(t)}{I_V(t) + 2I_H(t)} \quad (26)$$

For natural light excitation, direction of \mathbf{E} not defined

$$r_n(t) = \frac{I_V(t) - I_H(t)}{I_H(t) + 2I_V(t)} \quad (27)$$

$$r(t) = \frac{2p(t)}{3 - p(t)} \quad p(t) = \frac{3r(t)}{2 + r(t)} \quad (28)$$

$$r_n(t) = \frac{r(t)}{2} \quad p_n(t) = \frac{p(t)}{2 - p(t)} \quad (29)$$

$$r(t) = 2r_n(t) \quad p(t) = \frac{2p_n(t)}{1 - p_n(t)} \quad (30)$$

$$I_V(t) = \frac{1}{3}S(t)[1 + 2r(t)] \quad I_H(t) = \frac{1}{3}S(t)[1 - r(t)] \quad (31)$$

For an isotropic sample the ranges of variations for r and p , respectively, are given by

$$-0.2 \leq r \leq +0.4 \quad -0.33 \leq p \leq +0.5 \quad (32)$$

The total anisotropy due to i fluorophores characterized by r_i and contributing S_i to the total fluorescence is given by

$$r(t) = \frac{\sum_i r_i(t)S_i(t)}{\sum_i S_i(t)} \quad (33)$$

Steady state anisotropy is given by

$$\langle r \rangle = \frac{\int_0^\infty I_V(t) dt - \int_0^\infty I_H(t) dt}{\int_0^\infty I_V(t) dt + 2 \int_0^\infty I_H(t) dt} \quad (34)$$

For an isotropic rotator whose fluorescence emission decays monoexponentially, i.e., $r(t) = \beta e^{-t/\phi}$ and $S(t) = \alpha e^{-t/\tau}$, we have

$$\begin{aligned} I_V(t) &= \frac{1}{3}\alpha(1 + 2e^{-t/\phi})e^{-t/\tau} \\ I_H(t) &= \frac{1}{3}\alpha(1 - e^{-t/\phi})e^{-t/\tau} \end{aligned} \quad (35)$$

In this case the expression for r becomes

$$\langle r \rangle = \beta \frac{\phi}{\tau + \phi} \quad \frac{1}{\langle r \rangle} = \frac{1}{\beta} \left(1 + \frac{\tau}{\phi} \right) \quad (36)$$

This last expression is called the Perrin law. Perrin determined⁵⁴ that $\phi = \eta V/KT$, where η is the viscosity of the solvent, T its absolute temperature, V is the molecular volume, and K the Boltzman constant. Thus this law, valid only under the conditions stated above, becomes

$$\frac{1}{\langle r \rangle} = \frac{1}{r_0} \left(1 + \frac{KT\tau}{\eta V} \right) \quad (37)$$

where β , i.e., $r(t)$ at $t = 0$, has been called r_0 .

The expressions for the denominator in Eqs. (26) and (27) are based on the symmetry induced in the photo-selected system by the polarization characteristics of the exciting light. Note that in Eqs. (26)–(35) the time dependence has been made explicit. At each particular time $I_V(t)$ and $I_H(t)$ will be, respectively, proportional to the number of emitted photons having these particular directions of polarization. As shown below, under analysis of time-dependent emission anisotropy, each of these two curves contains all the necessary information for determining the decay law of the emission anisotropy. The only prerequisite is knowledge of the decay of total emission $S(t)$ which, in principle, can be determined separately. However, in all but the simplest case of the isotropic rotator, the number of parameters to be determined is such as to make the cross-correlation of the analyses for either $I_V(t)$ and $I_H(t)$ or for any combination of them, e.g., $D(t)$ and $S(t)$ a practical necessity. Therefore, the anisotropy measurements must start with the collection of both curves.

The time-dependence that will be observed in $I_V(t)$ and $I_H(t)$ depends primarily on three processes.

- a. The decay of the fluorescence emission.
- b. Brownian rotation of the emission dipoles \mathbf{e} randomizing the photo-selected subensemble; also intrinsic rotation of \mathbf{e} within the molecule which could be due to excited state reactions.
- c. Energy migration from the photo-selected subensemble to the nonselected molecules followed by emission from the latter; effectively this transfers the initial nonrandomness out of the photoselected subensemble and "dilutes" it in the whole.

Process (a) is characterized by the decay constants of the fluorophore. Its rate can be affected by the nature of the environment, i.e., solvent, temperature, viscosity, extent of solvation, and presence of foreign quenching substances. Brownian rotation (b) is mainly dependent on temperature, viscosity and the extent of solvation. Finally, the rate of energy migration is mainly controlled by the concentration of the fluorescent molecules and their relative orientations. While the rate of process (a) influences in an equal measure the rates of decay of both $I_V(t)$ and $I_H(t)$, the rates of processes (b) and (c) influence $I_V(t)$ and $I_H(t)$ in a differential

manner and are primarily responsible for the time dependence of the emission anisotropy. If processes (b) and (c) are absent, the system will exhibit an emission anisotropy constant in time. This is obtained, for instance in dilute, highly viscous solutions or when the fluorophores have their motion restricted by bilayer membranes containing them.⁵⁷⁻⁶⁰ The constancy in the last case is only relative and is due to the large discrepancy between the long time necessary for the whole membrane to rotate and the short nanosecond time window during which the fluorescence characteristics can be measured.

Time-dependent emission anisotropy measurements thus involve collection of *congruent* $I_V(t)$ and $I_H(t)$ fluorescence decay curves. These two curves are made congruent by contemporaneous collection or normalization.

a. Contemporaneous collection, i.e., during the same time interval, should ideally be used to eliminate any differential artifacts in the two decay curves due to long time drifts of the exciting flash and/or electronic circuitry. It can be performed in any of the following ways.

- i. Alternating the excitation polarizer orientation in front of a single fluorescent sample with emission detection through a fixed polarizer in front of a single photomultiplier⁶¹ or the reverse optical situation.
- ii. Fixed vertical and horizontal excitation polarizers rigidly attached to two alternating identical fluorescent samples; emission detection through a fixed emission polarizer in front of a single photomultiplier.⁵⁷
- iii. Fixed excitation polarizer in front of a single sample; emission detection through two fixed emission polarizers in front of two identical photomultipliers.

While procedure (iii) eliminates the necessity of mechanical alternation, it is our experience that matching identically the timing characteristics of two "factory identical" photomultipliers presents very difficult problems. In our laboratory procedure (ii) is used and some experimental details are presented below.

The alternation of the two identical fluorescent samples is performed as previously described (see section on instrumentation) by a computer-controlled turntable. Specifically, two identical cuvettes with double Polacoat filters rigidly attached are positioned alternately in the

⁵⁷ L. A. Chen, R. E. Dale, S. Roth, and L. Brand, *J. Biol. Chem.* **252**, 2163 (1977).

⁵⁸ K. Kinoshita Jr., S. Mitaku, and A. Ikegami, *Biochim. Biophys. Acta* **393**, 10 (1975).

⁵⁹ R. A. Dale, L. A. Chen, and L. Brand, *J. Biol. Chem.* **252**, 7500 (1977).

⁶⁰ W. R. Veatch and L. Stryer, *J. Mol. Biol.* **117**, 1109 (1978).

⁶¹ H. P. Tschanz and T. Binkert, *J. Phys. E.* **9**, 1131 (1976).

light path. The excitation light after passing through a quartz wedge scrambler plate is polarized vertically or horizontally by either one of the two Polacoat filters. The fluorescence is collected at 90° through a vertically oriented fixed double Polacoat filter. The emission wavelength can be selected by a computer-controlled monochromator. The third cuvette on the turntable contains the scattering Ludox solution. It is also provided with a rigidly attached excitation polarizer whose transmission axis is at 54.7° to the vertical (the so-called magic angle) in order to measure an excitation profile unbiased by polarization. Because the same photomultiplier views the scattered and the fluorescence light through the same fixed emission polarizer, the artifacts introduced by the detection train are, in principle, eliminated. The wavelength dependence of the photomultiplier transit time is dealt with as described under analysis.

(b) Normalization is necessary to eliminate any differential weighting in the two curves $I_V(t)$ and $I_H(t)$ of the artifacts associated with

- i. Intensity and frequency fluctuations of the exciting light
- ii. Anisotropy of the excitation train and/or detection train
- iii. Geometry of the excitation detection

The normalization process aims at equalizing the effect of these artifacts on the two decay curves. It consists of computing a total time-independent normalization factor by which one of the curves is scaled relative to the other. This factor is arrived at through a combination of hardware and software techniques.⁶²

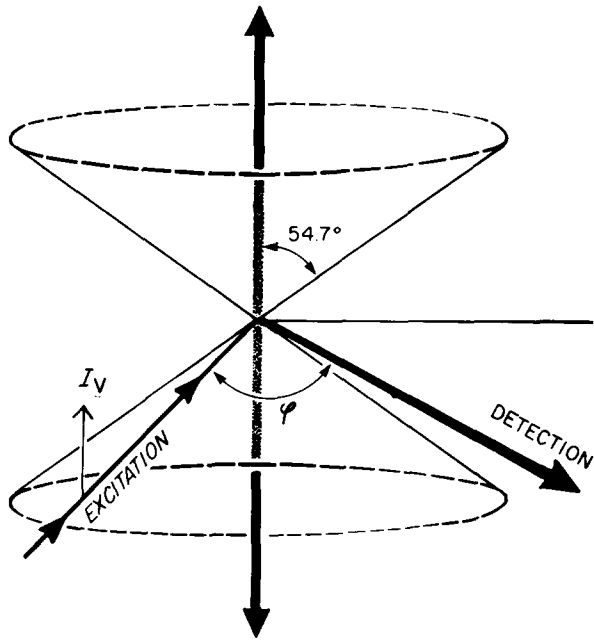
It is convenient to divide this total normalization factor into two partial ones to be determined in two separate steps: one to correct for the artifacts described under (i) and the other one to correct for those described under (ii) and (iii). First it should be noted that the artifacts (i) are practically eliminated when a contemporaneous collection procedure for the two curves $I_V(t)$ and $I_H(t)$ is used. In the case when a double check is desired or when such a capability is not available, one can monitor the number of TAC outputs n_V and n_H during the collection of the two curves. The partial normalization factor multiplying $I_H(t)$ is given by⁶³:

$$N_1 = \frac{\int_0^T I_V(t) dt}{\int_0^T I_H(t) dt} \frac{n_H}{n_V} \quad (38)$$

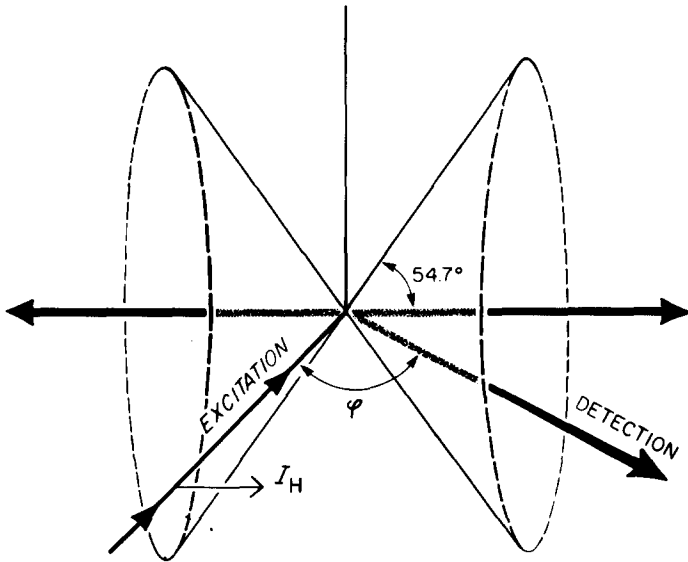
Alternatively one may use a monitoring photomultiplier to view the exciting flash¹³ or the fluorescence⁶¹ directly and count the numbers n_V and n_H .

⁶² C. E. Martin and D. C. Foyt, *Biochemistry* **17**, 3587 (1978).

⁶³ Ph. Wahl, *Biochim. Biophys. Acta* **175**, 55 (1969).



a



b

FIG. 14. "Magic" angle cones corresponding to (a) vertically polarized excitation, (b) horizontally polarized excitation; φ is the angle the detection direction makes with the excitation.

In the pulse sampling fluorometers this correction is automatically performed in the instantaneous ratio taking mode.¹³

The partial normalization factor for the artifacts under (ii) and (iii) can only be determined in a separate experiment during which the first factor is also computed. It is based on the observation that excitation with horizontally polarized light creates a symmetric axis in the photo-selected system (Fig. 14) coincident with the detection direction (in the usual 90° geometry). Thus, the intensity of the fluorescent light detected through a polarizer should be independent of the rotation of the latter in a plane perpendicular to the direction of detection. If this is not true, a normalization factor for $I_H(t)$, called G factor, is defined by

$$N_2 = G_{\text{for H excitation}} = \frac{\int_0^T I_V(t) dt}{\int_0^T I_H(t) dt} \neq 1 \quad (39)$$

Note that this normalization factor does not correct for the partial polarization that may be present in the lamp flash. For this reason a depolarizer, quarter wave scrambler plate is usually inserted in front of the excitation interference filter.

The new $I'_H(t)$ obtained by multiplying the experimentally determined $I_H(t)$ by $N = N_1 \times N_2$ is congruent with the $I_V(t)$. Thus we have

$$I'_H(t) = I_H(t)N_1N_2 \quad \text{and} \quad r(t) = \frac{I_V(t) - I'_H(t)}{I_V(t) + 2I'_H(t)} \quad (40)$$

Alternate Determinations of the Normalization Factor

As described above the normalization factor can be determined in two separate steps. The product of the partial factors gives the total one. Alternate determinations have been used^{57,64} in which the total factor is obtained in one step. Their limitations will be pointed out below.

a. *Tail edge matching* is a procedure whereby the two curves $I_V(t)$ and $I_H(t)$ are scaled relative to one another until their tails coincide. It is based on the assumption that the randomization of the photoselected subensemble is practically achieved at a particular point in time. After that the decay of the emission alone is represented in both curves. This method could lead to substantial errors because the curves are matched in a region where the intensity is very low such that the random noise or any systematic errors could predominate. Additional error may be introduced

⁶⁴ G. R. Fleming, J. M. Morris, and G. W. Robinson, *Chem. Phys.* 17, 91 (1976).

by starting the normalization too early in the decay when complete randomness is not yet achieved.

b. *Steady state normalization* is based on the separate determination of the steady state emission anisotropy. In this method the time integrated values of $I_V(t)$ and $I_H(t)$ are used to determine a *truncated* value of the steady state emission anisotropy with the normalization constant α as a variable parameter. By identifying this truncated value with the actual steady state emission anisotropy value measured separately with a continuous source of light, the value of the parameter is fixed. Thus

$$\langle r \rangle_{\text{truncated}} = \frac{\int_0^T I_V(t) dt - \alpha \int_0^T I_H(t) dt}{\int_0^T I_V(t) dt + 2\alpha \int_0^T I_H(t) dt} \quad (41)$$

and

$$\langle r \rangle = \frac{\int_0^\infty I_V(t) dt - \int_0^\infty I_H(t) dt}{\int_0^\infty I_V(t) dt + 2 \int_0^\infty I_H(t) dt} \quad (42)$$

If we identify $\langle r \rangle_{\text{truncated}}$ with $\langle r \rangle$ the value of the normalization constant, α , is given by

$$\alpha = \frac{1 - \langle r \rangle \int_0^T I_V(t) dt}{1 + 2\langle r \rangle \int_0^T I_H(t) dt} \quad (43)$$

It is our experience that in order to be able to make this identification accurately, the decay of the two curves $I_V(t)$ and $I_H(t)$ should be followed and integrated over 2.5 to 3 decades. It is also preferable to measure $\langle r \rangle$ with the same instrument used for collecting the two curves. A continuous lamp may replace the flash lamp, and thus the artifacts associated with the geometry of collection are equally represented in $\langle r \rangle_{\text{truncated}}$ and $\langle r \rangle$.

Analysis of Time-Dependent Emission Anisotropy Measurements

In order to obtain valid results the convolution related artifacts should be eliminated from the two normalized decay curves $I_V(t)$ and $I_H(t)$. As described previously (see section on analysis of decay curves) this can be accomplished by a variety of procedures. Since either $I_V(t)$ or $I_H(t)$ contain

all the desired information, they could be separately deconvolved and analyzed in terms of a multiexponential model. Correlation of these two analyses improves the accuracy.

Thus, in the simplest case of an isotropic rotator characterized by a single rotational relaxation time ϕ and emitting a monoexponentially decaying fluorescence with lifetime τ , theory predicts that

$$I_V(t) = \frac{1}{3}S(t)[1 + 2r(t)] = \frac{1}{3}\alpha e^{-t/\tau} + \frac{2}{3}\alpha\beta e^{-t(1/\tau + 1/\phi)} \quad (44)$$

$$I_H(t) = \frac{1}{3}S(t)[1 - r(t)] = \frac{1}{3}\alpha e^{-t/\tau} - \frac{1}{3}\alpha\beta e^{-t(1/\tau + 1/\phi)} \quad (45)$$

where $S = I_V + 2I_H$ is a measure of the total intensity emitted by the sample in all directions which in this case is given by $S(t) = \alpha e^{-t/\tau}$ and $r(t)$ is the decay of the emission anisotropy which for an isotropic rotator is given by $r(t) = \beta e^{-t/\phi}$. It is seen that separate deconvolution of $I_V(t)$ and $I_H(t)$ should yield the same two exponentials in both curves. The negative preexponential term in $I_H(t)$ should be two times larger and positive in $I_V(t)$. The other two corresponding preexponentials should be the same.

The correlation of the two separate analyses for $I_V(t)$ and $I_H(t)$ which, in principle, is redundant is found to be, in practice, indispensable for an adequate analysis. Moreover, the extension of this method to other analytical expressions for $r(t)$ (e.g., a two-exponential decay) although possible becomes considerably less reliable. Alternate methods of analysis become necessary. At the time of writing, the method of choice consists of analyzing the sum and difference curves^{57,63} obtained from the normalized convoluted $I_V(t)$ and $I_H(t)$ curves and given by

$$\begin{aligned} S(t) &= I_V(t) + 2I_H(t) \\ D(t) &= I_V(t) - I_H(t) \end{aligned}$$

and thus

$$r(t) = D(t)/S(t)$$

The curve $S(t)$ contains only terms describing the decay of the total emission independent of the model assumed for $r(t)$. It can also be obtained independently when the transmission axis of the excitation and emission polarizers are at an angle of 54.7° . The deconvolved impulse of $S(t)$ obtained as a sum of exponentials is multiplied by an assumed empirical form for $r(t)$ usually given by

$$r(t) = \sum \beta_i e^{-t/\phi_i} + c \quad (46)$$

The significance of c can be understood through a limiting process: one of the empirical rotational relaxation time ϕ_i is large enough such that its exponential term is practically constant in the limited nanosecond time in-

terval during which the collection of the emitted light is possible. The multiplication of $r(t)$ by the deconvolved $S(t)$ gives the new multiexponential model to be used in the deconvolution of $D(t)$. As a result the variable parameters of $r(t)$ β_i , ϕ_i , and c are fixed.

This method of analysis has been found to be more accurate than separate analysis of $I_V(t)$ or $I_H(t)$. The curve $S(t)$ is deconvolved with a multiexponential model containing only terms describing the decay of total emission, and $D(t)$ with a similar model which contains one term less than either polarized component [see Eqs. (24) and (25)].

From Nanosecond Fluorometry to Mechanisms

Magic Angle: Elimination of Polarization Bias. Before any attempt is made to extract information about the molecular characteristics of a fluorescent system, one should carefully consider the effects of the inherent photo-selection process. Fluorescence emission originates from a photo-selected ensemble of fluorophores which become excited following absorption. This set of molecules has an orientational distribution of emission dipoles different from that characterizing the bulk of molecules in the ground state. This is due to a greater probability of photon absorption as the angle between the molecular absorption dipole and the photon polarization vector approaches zero (probability of absorption is proportional to $\cos^2 \theta$). Thus, the excited molecules are selected from an isotropic random system by the anisotropic character of the excited light. It is important to note that photo-selection will occur in a three-dimensional system even if excitation is performed with natural light because the possible orientations of the exciting electric vector are confined to two dimensions.

The intensity and polarization characteristics emitted by such a nonrandom, photo-selected ensemble will be highly dependent upon the polarization of the exciting light, the wavelength-dependent orientation of molecular absorption and emission dipoles, and the spatial direction of fluorescence detection.

The dependence, however, is modulated by the relative magnitude of rotational relaxation and fluorescence decay times. If the former are much smaller than the latter, the photo-selection memory will be lost prior to light emission. As the ratio of the average rotational relocation time to the average fluorescence decay times increases the emission will reflect the photo-selection to an increasing extent. Thus any comparative series of fluorescence measurements (both steady state and/or transient) in which either this ratio or the parameters mentioned are altered will not be congruent.

A common example of such potentially erroneous comparative measurements is provided by the collisional quenching experiments in which

the gradual addition of quencher affects the ratio by shortening the decay time of the excited state. Other examples have been discussed in the literature where it has been estimated that deviations up to 20% may be introduced into the experimental data.⁶⁵⁻⁶⁷

It is thus evident that in order to compare or to extract relevant information from fluorescence data it is necessary to eliminate this variability associated with the photo-selection process, namely, one should measure signals proportional to the total fluorescence which, by definition, is independent of the spatial directionality of fluorescence emission. It reflects only the number of the emitting fluorophores, their probability of emission being proportional to the product of these quantities.

By definition

$$I_{\text{total}} = I_x + I_y + I_z$$

where x , y , z are any three mutually orthogonal directions in space. It is desirable to measure a signal proportional to this sum along one single direction of detection. This direction is determined solely by the symmetry created in the emitting system through the photo-selection process. A linear polarized excitation will be absorbed preferentially by those molecules whose absorption dipole moments make smaller angles with the polarization direction. This being the only preferential direction in an isotropic system it becomes the symmetry axis. For instance, suppose that excitation is vertically polarized (let us call this axis x). Then all directions perpendicular to it will be equivalent (i.e., $I_y = I_z$) and I_{total} is given by

$$I_{\text{total}} = I_x + I_y + I_z = I_x + 2I_y$$

Thus, if one views the fluorescence signal at a particular angle to the symmetry axis which weights the perpendicular component twice as much as the one along the axis then a signal proportional to the total fluorescence will be detected. The weighting factors for the two components are the squared cosines of the respective angle they make the viewing (detection) direction. With θ the angle between the symmetry axis and the viewing direction, we have

$$I_{\text{viewed}} = I_x \cos^2 \theta + I_y \cos^2 (90^\circ - \theta)$$

and I_{viewed} will be proportional to I_{total} if

$$\frac{\cos^2 (90^\circ - \theta)}{\cos^2 \theta} = \tan^2 \theta = 2 \quad \theta = 54.7^\circ$$

The ensemble of viewing directions that satisfy this condition will form a cone as showed in Fig. 14 with half-angle 54.7° having the symmetry axis

⁶⁵ A. H. Kalantar, *J. Chem. Phys.* **48**, 4992 (1968).

⁶⁶ M. Shinitzky, *J. Chem. Phys.* **56**, 5979 (1972).

⁶⁷ K. D. Mielenz, E. D. Cehelnik, and R. L. McKenzie, *J. Chem. Phys.* **64**, 370 (1976).

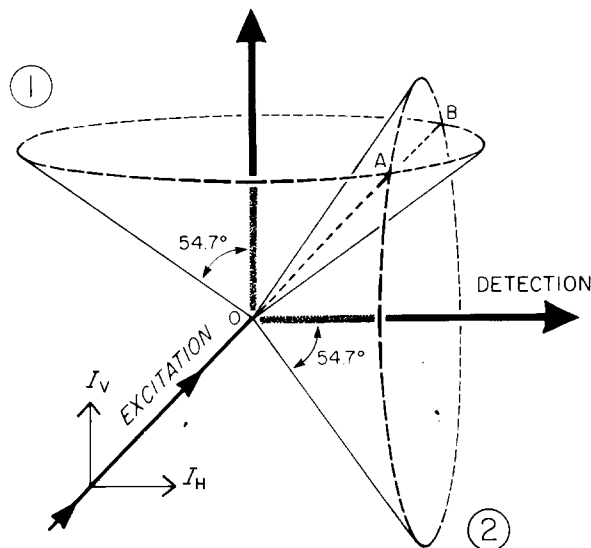


FIG. 15. "Magic" angle cones. Viewing the emission originating from O along the lines BO or AO eliminates the polarization related artifacts for any kind of excitation. See text for details.

parallel to the polarization direction of the exciting radiation and the apex in the center of the cuvette containing the fluorescent sample.

If the excitation is performed with natural light, i.e., all directions of polarization equally probable and confined to the plane perpendicular to the direction of excitation, then the transitive dipole moments of the photo-selected molecules will be symmetrically distributed around this latter direction. The excitation direction becomes the symmetry axis of the photo-selected system. The "magic" angle 54.7° should be considered relative to it, and consequently it becomes the axis of the cone formed by the ensemble of viewing directions along which one measure a fluorescence signal proportional to the total emission.

The general case in which one has a combination of the partially polarized and unpolarized excitation could be approached in a similar manner. Any light signal can be thought of being composed of two polarized beams, one vertical and the other horizontal coherently or incoherently superimposed. The viewing directions along which the effect due to the vertically polarized beam is eliminated form the cone labeled 1 in Fig. 15; those corresponding to the horizontally polarized beam form the cone labeled 2 in Fig. 15. Along the lines of intersection of the two cones, OA and OB, one views a fluorescence signal free from any polarization related artifacts.

A closer look at Fig. 15 reveals that the "right" (in the sense described

above) directions of detection are quite difficult to adopt in the usual constraints of the 90° geometry built in many spectrophotometers.

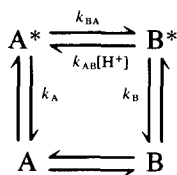
One simple observation comes to the rescue. The transmission axis of the detection polarizer is equivalent to a viewing direction. Thus one only has to align the transmission axis of the detection polarizer parallel to the lateral surface of the proper cone determined by the excitation. An infinite number of combinations exist. In the confines of the 90° geometry three combinations are commonly used.

- a. Vertically polarized excitation; detection with transmission axis of the polarizer at 54.7° to the vertical
- b. Natural light excitation (scrambler plate); detection with transmission axis of the polarizer at 35.3° to the vertical
- c. The optical reverse of the combinations (a) and (b)

Excited State Interactions: Limiting Cases. It is not our aim here to discuss in any detail the numerous excited state processes that are now well characterized both theoretically and experimentally.⁶⁸ Since the rationale behind experiments using nanosecond decay techniques is to obtain information regarding these interactions, it is worthwhile indicating some characteristics of the decay data that may be used to advantage.

A simple chromophore in dilute solution is expected to show single-exponential decay kinetics. This is probably more the exception than the rule. Double-exponential decay behavior is very commonly observed. This may have its origin in a mixture of two ground state species. This can sometimes be detected by a variation of the emission spectrum or the decay parameters with exciting wavelength. In some cases, the absorption and emission spectra of a chromophore may be quite similar but the fluorescence lifetimes may differ. This is certainly possible with chromophores associated with macromolecules and provides a powerful approach for investigating microheterogeneity in macromolecular systems.

Double-exponential decay kinetics may also have their origin in excited state reactions, even if only one chromophoric species exists in the ground state. A general scheme for a two-state system which provides for ground state equilibria and an excited state reaction which may be reversible or irreversible is shown below.



⁶⁸ J. B. Birks, ed., "Organic Photophysics," Vols. I and II. Wiley, New York, 1973.

This scheme is written for an excited state dissociation such as excited state deprotonation. In the reverse reaction a proton can add on, reforming A^* . An example of a system showing this type of behavior is found with 2-naphthol. Depending on the pH, a significant ground state equilibrium may exist between A and B. Let us assume that the only significant ground state species is A. Excitation will lead to production of A^* . In the case of 2-naphthol, the energetics of the excited state now favor formation of B^* . (For 2-naphthol $pK = 9.5$, while $pK^* = 2.8$). At very high hydrogen ion concentration the reverse reaction will predominate and essentially no B^* will be formed. Under these conditions the rate equation for A^* is

$$-\frac{d(A)^*}{dt} = k_A(A^*)$$

where k_A includes terms both for radiation and quenching. At very acid pH the decay of 2-naphthol is well described by a monoexponential decay law.

At intermediate H^+ concentrations, the excited state reaction becomes kinetically significant and fluorescence due to A^* and B^* is observed, although only A exists to a significant extent in the ground state. At sufficiently low hydrogen ion concentrations ($pH > 5$ in the case of 2-naphthol) the back-reaction indicated by $k_{AB}[H^+]$ becomes negligible. Under these conditions the rate equation for A^* is

$$dA^*/dt = (k_A + k_{BA})A^*$$

Once again the decay of A^* is represented by a single exponential decay law. As is indicated below, the decay of B^* is described by a double-exponential decay law under these conditions.

Thus the hallmark of a two-state reversible excited state reaction is that in general the decay of A^* and B^* are *both* characterized by a double-exponential decay law with the *same* decay constants for A^* and B^* .

The rate equations are

$$\frac{-d[A^*]}{dt} = (k_A + k_{BA})[A^*] - k_{AB}[H^+][B^*] \quad (47)$$

$$\frac{-d[B^*]}{dt} = (k_B + k_{AB}[H^+])[B^*] - k_{BA}[A^*] \quad (48)$$

It follows that the decay of A^* , B^* is

$$A^*(t) = \alpha_1 e^{-t/\tau_1} - \alpha_2 e^{t/\tau_2} \quad (49)$$

$$B^*(t) = \beta_1 e^{-t/\tau_1} - \beta_2 e^{-t/\tau_2} \quad (50)$$

Note that the identical decay constants appear in both cases and that the decay of B* has preexponential terms that are equal in magnitude but opposite in sign

$$\tau_1^{-1}, \tau_2^{-1} = \gamma_1, \gamma_2 = \frac{1}{2}[(X + Y) \mp \{(Y - X)^2 + 4k_{BA}k_{BA}k_{AB}[H^+]\}^{1/2}] \quad (51)$$

where $X = k_A + k_{BA}$, $Y = k_B + k_{AB}[H^+]$, and

$$\gamma_1 + \gamma_2 = (X + Y) = k_A + k_{BA} + k_B + k_{AB}[H^+]$$

Thus decay curves of either A* or B* can be obtained at various pH, and a plot of $(\gamma_1 + \gamma_2)$ versus pH can be used to obtain the reverse rate constant k_{AB} .

It can also be shown that

$$\gamma_1\gamma_2 = k_B X + k_A k_{AB}[H^+] \quad (52)$$

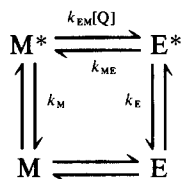
Thus

$$\gamma_1 + \gamma_2 = k_A + k_{BA}(1 - k_B/k_A) + \gamma_1\gamma_2/k_A \quad (53)$$

Thus in a graph suggested by DeToma⁶⁹, a plot of $(\gamma_1 + \gamma_2)$ versus $\gamma_1\gamma_2$ yields a slope equal to $1/k_A = \tau_A$ and an intercept = $k_A + k_{BA}(1 - k_B/k_A)$.

Once k_A is known, k_{BA} can be calculated from the decay of A* under irreversible conditions.

Quite analogous relationships obtain for a two-state excited state reaction involving complex formation in the excited state. Examples of reactions of this type include excimer formation, exciplex formation, or excited state proton addition reactions with heterocyclic molecules such as acridine. The appropriate scheme is indicated below.



Once again, generally a double exponential decay will be observed at wavelengths where either species M or E emit. Equations (1)–(6) still apply with [Q] replacing $[H^+]$.

A plot of $\gamma_1\gamma_2$ versus $\gamma_1 + \gamma_2$ is linear with a slope $1/k_E = \tau_E$ and an intercept = $k_E + k_{ME}(1 - k_M/k_E)$.

The excited state solvation dynamics of 2-anilino-naphthalene (2 AN) show kinetic behavior that under suitable conditions, are in accord with this scheme.⁶⁹ Figure 16 shows the results obtained when increasing con-

⁶⁹ R. P. DeToma and L. Brand, *Chem. Phys. Lett.* **47**, 231 (1977).

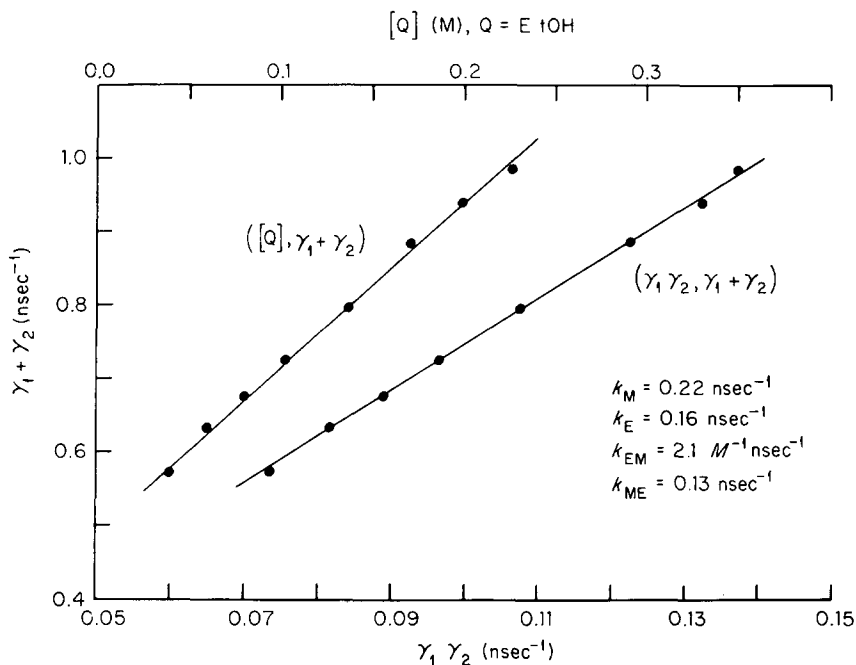


FIG. 16. Kinetic plots for a two-state reversible excited-state reaction. The data is for 2-anilino-naphthalene in cyclohexane with addition of ethanol in the range 0 to 0.35 M.

centrations of ethanol are added to 2 AN dissolved in cyclohexane. Both $\gamma_1 + \gamma_2$ versus $\gamma_1 \gamma_2$ and $\gamma_1 + \gamma_2$ versus Q are straight lines as predicted and the rate constants indicated are obtained from the slopes and intercepts. It can be anticipated that a large number of excited state dissociation or association reactions will fit into excited state reversible or irreversible class. These reactions can be recognized by the fact that the reversible reactions will show double-exponential decay behavior with decay times independent of emission wavelength (since A^* and B^* or M^* and E^* show the same decay times) but dependent on the forward and reverse rates of the reaction. In addition the preexponential terms of B^* , the product formed by dissociation will be equal in magnitude but opposite in sign. In the case of an irreversible excited state reaction the decay of the initially excited species (A^* or M^*) will be described by a single exponential.

There can be little doubt that as instrumentation for measurements in the nanosecond time domain become readily available, more complex excited state reaction schemes will be unraveled. The fluorophore, 2-naphthol-1-acetic acid, may be cited as an example of a system showing

emission from *more* than two excited species.⁷⁰ Systems can be envisioned where a proton transfer reaction might be followed by a solvation reaction. Detailed lifetime measurements on energy transfer systems where the decay laws of donor and acceptor will depend on relative distances, orientations and nanosecond motions remain to be done. Ware and Nemzek⁷¹ have investigated transient effects (time-dependent rate constants) in diffusion controlled reactions. These are likely to be important in biochemistry and will lead to complex decay laws. As the level of complexity increases it may not always be possible to determine values for all the rate constants. The decay measurements would be of value for obtaining evidence for or against a particular reaction mechanism.

Emission from two excited states represents a straightforward situation about which detailed information can be obtained. We now conclude this discussion by describing the other limit where emission appears to take place from a continuum of excited states. This situation appears to prevail for some excited state solvation reactions. Fluorescence decay data obtained with *N*-arylamino-naphthalene sulfonates adsorbed to liposomes,²⁴ adsorbed to some proteins⁴⁹ or dissolved in a viscous solvent⁵¹ can be summarized in the following way.

The fluorescence emission spectra shift to lower energy with time (nano-seconds) with little or no change in band shape. The fluorescence intensity also decreases with time at all wavelengths. The combination of the band shift *and* the damping result in a complex nonexponential pattern of fluorescence decay at various emission wavelengths. While at first sight it might appear that only qualitative information can be obtained, this data can be treated according to a theory developed by Bakhshiev and his co-workers⁷² to describe general excited state solvent relaxation. Their treatment represents the steady state fluorescence emission spectrum as a superposition of the elementary time-dependent spectra which evolve from some initial state that is continuously shifting in time to lower energy and is being damped at the same time. This phenomenon may be expressed in terms of the nonexponential decay law⁵¹ indicated by Eq. (54).

$$I(\bar{\nu}, t) = i(t)\rho(\bar{\nu}, t) = i(t)\rho[\bar{\nu} - \bar{\nu}_{\max}(t)] \quad (54)$$

$I(\bar{\nu}, t)$ is the data matrix for a time-resolved emission spectra obtained as described above. $I(\bar{\nu}, t) = F(\bar{\nu}, t)$ normalized to the corrected steady-state fluorescence spectra obtained with the same instrument.^{49,51} This treatment allows the determination of an important new parameter defining the system, $i(t)$.

⁷⁰ A. Gafni, R. L. Modlin, and L. Brand, *J. Phys. Chem.* **80**, 888 (1976).

⁷¹ W. R. Ware and T. L. Nemzek, *Chem. Phys. Lett.* **23**, 557 (1973).

⁷² N. G. Bakhshiev, N. G. Mazurenko, and I. Y. Piterskaya, *Opt. Spectrosc. (USSR)* **21**, 307 (1966).

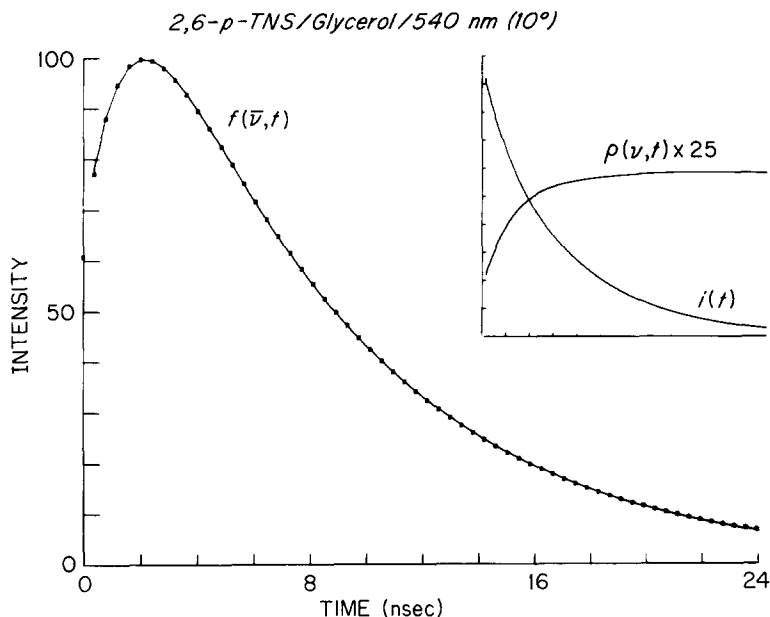


FIG. 17. The fluorescence decay of 2,6-*p*-TNS in glycerol at 540 nm at 10°. The inset at the upper right shows the breakdown of the fluorescence decay into the double-exponential damping function $i(t)$ and the wavelength-dependent shift function $\rho(\bar{\nu}, t)$.

This quantity is determined from the TRES data matrix (see Fig. 11) as follows: $\rho(\bar{\nu}, t)$ is first obtained as a function of t at each $\bar{\nu}$ by normalizing each "time slice" of the complete surface $I(\bar{\nu}, t)$ to constant emitted quanta and extracting the numeric values of $\rho(\bar{\nu}, t)$ at each $\bar{\nu}$. Once $\rho(\bar{\nu}, t)$ and $I(\bar{\nu}, t)$ are known, $i(t)$ can be determined. An example of this treatment is shown in Fig. 17 which shows data for 2,6-toluidinonaphthalene sulfonate (2,6-*p*-TNS) dissolved in glycerol. The deconvolved decay curve $F(\bar{\nu}, t)$ (designated as $f(\bar{\nu}, t)$) shows an initial rise indicating that a portion of the emission is due to species created in the excited state. The inset in the upper right shows $\rho(\bar{\nu}, t)$ at this wavelength and the derived damping term $i(t)$. $i(t)$ in this case can be described in terms of a double-exponential decay law. $\rho(\bar{\nu}, t)$ depends on $\bar{\nu}$ and is a complex function which depends on the kinetics of the spectral shift and the emission contour of the system. A nonlinear least squares algorithm was used to obtain $i(t)$ from $\rho(\bar{\nu}, t)$ and $F(\bar{\nu}, t)$ assuming that it could be expressed as a sum of exponential terms.

This treatment has been applied to several systems such as *N*-arylamino-naphthalene dyes adsorbed to a protein or liposomes. It should be pointed out that while the ability to analyze data in terms of this

formulation does not *prove* any particular excited state molecular mechanism, it does require that a proposed mechanism be consistent with the phenomenological formulation. Of particular importance is the fact that the terms $i(t)$ and $\bar{\nu}_{\max}(t)$ may be compared between different systems or as a function of intensive parameters such as temperature and pressure. Thus what might at first appear to be a nonanalyzable pattern of decay curves as a function of emission wavelength may in fact be categorized and subjected to further study.

Summary

Nanosecond fluorescence measurements can now be routinely performed and the data can be analyzed in terms of specified decay laws. It is anticipated that nanosecond fluorometry will continue to aid in the elucidation of a variety of excited state mechanistic pathways. This in turn will result in the more sophisticated use of fluorescence probes in biochemistry and cell biology.

At the beginning of this decade, Ware⁹ indicated that the ideal decay fluorometer should permit measurements with samples where the absorbance quantum yield product is 10^{-10} , with high spectral resolution and picosecond time resolution over a wide spectral range. Many of the requirements which seemed so stringent then have now been met. It is likely that the next review on rapid decay techniques will be able to show that picosecond experiments can be carried out with the same degree of confidence that is now possible on the nanosecond time scale.

Acknowledgments

Portions of the work described in this report were supported by NIH grant No. GM 11632. One of us (L.B.) wishes to thank Drs. J. R. Gohlke, M. Loken, J. H. Easter, R. Dale, R. P. DeToma, L. Chen, A. Gafni and A. Grinvald for their collaboration in nanosecond fluorometry. This is Contribution No. 989 from the McCollum-Pratt Institute.

[18] Low Frequency Vibrations and the Dynamics of Proteins and Polypeptides

By WARNER L. PETICOLAS

I. Introduction

Proteins are large molecules which usually contain between 500 and 3000 atoms. As a result, they must have, by the laws of physics, between 1500 and 9000 (i.e., $3N$) normal vibrations. Six of these will be quasivibra-